Nanostructured Lipid-Based Films for Substrate-Mediated Applications in Biotechnology

Minjee Kang, Mohit Tuteja, Andrea Centrone, Daniel Topgaard, and Cecilia Leal*

Amphiphilic in nature, lipids spontaneously self-assemble into a range of nanostructures in the presence of water. Among lipid self-assembled structures, liposomes and supported lipid bilayers have long held scientific interest for their main applications in drug delivery and plasma membrane models, respectively. In contrast, lipid-based multilayered membranes on solid supports only recently begin drawing scientists' attention. Current studies show that the stacking of multiple bilayers on a solid support yields cooperative structural and dynamic behavior that enables new functionalities. Lipid films provide compartmentalization, templating, and enhanced release of molecules of interest. Importantly, supported lipid phases exhibit long-range periodic nanoscale order and orientation that is tunable in response to a changing environment. Herein, the current understanding of lipid-based film research is summarized focusing on how unique structural characteristics enable the emergence of new applications including label-free biosensors, macroscale drug delivery, and substrate-mediated gene delivery. The authors' recent contributions focusing on the structural characterization of lipid-based films using small-angle X-ray scattering and atomic force microscopy are highlighted. In addition, new photothermally induced resonance and solid-state nuclear magnetic resonance data are described, providing insights into drug partition in lipid-based films as well as structure and dynamics at the molecular scale.

1. Introduction

Lipids are the primary components of plasma membranes that are composed of a hydrophilic polar headgroup and

M. Kang, Prof. C. Leal
Department of Materials Science and Engineering
University of Illinois at Urbana–Champaign
Urbana, IL 61801, USA
E-mail: cecilial@illinois.edu
Dr. M. Tuteja, Dr. A. Centrone
Center for Nanoscale Science and Technology
National Institute of Standards and Technology
Gaithersburg, MD 20899, USA
Dr. M. Tuteja
Maryland Nanocenter
University of Maryland
College Park, MD 20742, USA
Prof. D. Topgaard
Division of Physical Chemistry
Center of Chemistry and Chemical Engineering
Lund University
Lund 22100, Sweden

The ORCID identification number(s) for the author(s) of this article can be found under https://doi.org/10.1002/adfm.201704356.

hydrophobic tail(s). The lipid bilayer of plasma membranes separates the intracellular components from the external environment, encapsulates membrane proteins, and selectively permeates ions or molecules of interest. Specifically, the plasma membrane's capabilities to sense, detect, and transport specific species have fascinated scientists, leading to active research on functional lipid bilayers.[1–3] Enclosed lipid bilayers in an aqueous solution (termed lipid vesicles or liposomes) have been extensively used as "carriers" for drug and gene delivery based on their ability to encapsulate both hydrophilic and lipophilic molecules into different compartments.[4–7] Lipid bilayers supported onto a solid surface (also known as supported lipid bilayers) also have been widely used as plasma membrane models to study basic cellular processes such as lipid–protein interactions.[8–10]

Although flat lipid bilayers are the most abundant arrangement of lipids found in nature, different types of lipids can self-arrange into various morphologies of increasing complexity such as micellar, 2D hexagonal, and 3D bicontinuous cubic phases.[11–13] Bicontinuous phases comprise lipid bilayers curved as periodic minimal surfaces with cubic symmetry; the details of this particular lipid structure are discussed in Section 2.3.1. The ability of lipids to assemble into diverse structures (termed lipid polymorphism) has attracted considerable attention because of the unique phase-dependent properties that it enables. Lipid bicontinuous cubic phases, for example, exhibit high internal surface area per volume (≈ 400 m^2 g^{-1})[14] that enables high loading and/or fast release of drug molecules or genes.[15,16] In addition, the membrane geometry of the lipid cubic phase (negative Gaussian membrane curvature) promotes endosomal fusion and concomitant efficient small interfering RNA (siRNA) release and gene knockdown (decrease in gene expression).[17,18] Finally, because lipid cubic phases are optically isotropic, this property can be leveraged to detect certain biomarkers that induce optical birefringence (orientation-dependent, anisotropic refractive index).[19]

Lipid polymorphism has been leveraged for constructing stimuli-responsive self-assembled systems where manipulation of the lipid phases enables "on-demand" release of encapsulated agents.[15,20,21] Examples include ultrasound-triggered reversible phase transitions between different liquid crystalline lipid phases that regulate the diffusion rates of drug molecules[20]

**ADVANCED
SCIENCE NEWS**
www.advancedsciencenews.com

**ADVANCED
FUNCTIONAL
MATERIALS**
www.afm-journal.de

and pH-triggered phase transitions from a lamellar into an inverted hexagonal phase under acidic conditions which helps delivering the drug payload of lipid vesicles into the cytoplasm.[22] Despite the exciting properties rendered by lipid polymorphism, most studies exploiting lipid polymorphism have been dedicated to lipid particulate systems.

However, recent studies have shown that lipid polymorphism can be extended to lipid assemblies confined onto surfaces.[23–25] Research on supported lipid films and aspects of surface-mediated phase transitions are still in an early stage of research partly because studies of supported lipid systems have been mostly limited to model membranes where a single bilayer on a solid surface is sufficient to mimic most cellular membranes.

It should be noted that there is a growing interest to develop implantable macroscale drug delivery devices,[26,27] high throughput biosensing systems,[28–30] and substrate-mediated drug/gene delivery.[31,32] Advances in biotechnology such as surface-patterning techniques,[33–35] along with microfluidics[36–38] and biodegradable organic electronics,[39,40] have enriched research on the aforementioned applications. Following this trend, the need for biointerface membranes adsorbed onto solid substrates that serve as matrices or scaffolds and that are capable of exerting spatiotemporal control over the release of payloads is rapidly rising.[41,42]
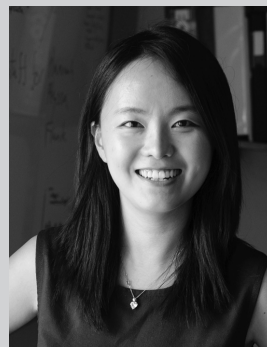
The purpose of this review is to highlight the potential of lipid films as emerging materials in substrate-mediated biotechnological devices. Several review articles are available on systems comprising a single lipid bilayer supported on a solid substrate. For comprehensive insights into this subject see refs. [9,10,43,44]. Concerning review articles on film structure characterization techniques, consult refs. [45–47].

The first part of the review covers aspects of lipid films placed into three categories: supported lipid bilayers, lipid multilamellar films, and lipid nonlamellar films. The section of nonlamellar lipid films describes the phase behavior of supported systems highlighting unanswered questions in phase transformation mechanisms, followed by potential applications enabled by their highly adaptable behavior in response to changing environmental conditions (e.g., humidity and temperature). The second part of the review summarizes the research on novel lipid–polymer composite membranes on solid supports that have been very recently developed.[48–51] These advances on hybrid films composed of self-assembled polymers and lipids are discussed emphasizing functionalities that are not attainable with nonhybrid systems. We give special focus to new data on structure and dynamics at the molecular scale obtained by solid-state NMR as well as identification of drug partitioning in lipid–polymer films inferred by photothermal-induced resonance data.

Minjee Kang is in the final year of the Ph.D. program in materials science and engineering at the University of Illinois, Urbana–Champaign (Prof. Cecilia Leal's Lab). She received her bachelor's degree in 2012 from Pohang University of Science and Technology, South Korea. Her research focuses on exploring the self-assembly behavior of lipids and amphiphilic block copolymers. She is interested in understanding the structures and interactions of these materials leading to their application in medicine and biotechnology.

Daniel Topgaard is a Professor of Physical Chemistry at Lund University, Sweden. His primary research interest is development of magnetic resonance methods for investigating structure and dynamics of soft matter. He received his Ph.D. from Lund University and was a postdoct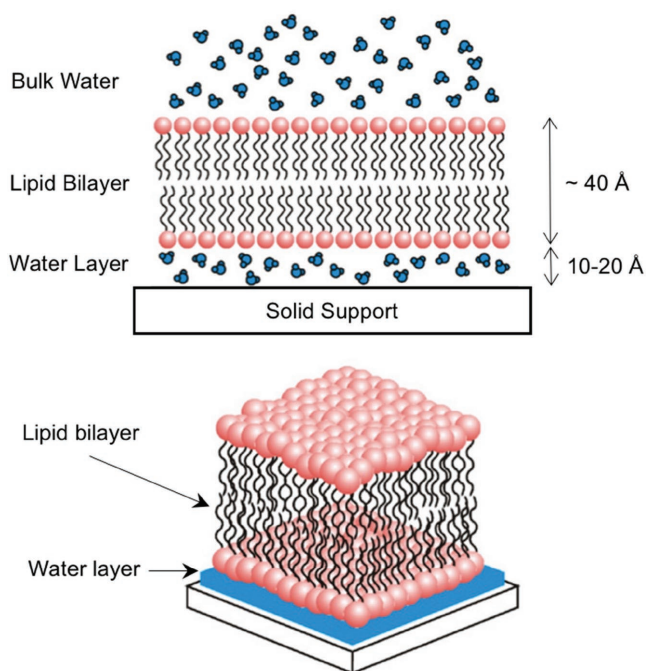oral fellow at the Materials Sciences Division, Ernest Orlando Lawrence Berkeley National Laboratory, and the Department of Chemistry, University of California, Berkeley. His innovations in the field of magnetic resonance imaging are commercialized by CR Development AB, Sweden.

Cecilia Leal is an Assistant Professor of Materials Science and Engineering at the University of Illinois, Urbana–Champaign since 2012. Her research interests focus on structures and interactions of soft matter that can be functionalized to operate as therapeutic or biotechnological devices. Cecilia received her Ph.D. in physical chemistry from the University of Lund, Sweden, and was a postdoctoral fellow for 3 years at the group of Prof. Safinya at the University of California, Santa Barbara.

2. Lipid Membranes

2.1. Supported Lipid Bilayers (SLBs)

Figure 1 shows a schematic illustration of a supported lipid bilayer. The deposition of a lipid bilayer onto hydrophilic solid substrate leaves a thin water layer (1–2 nm thick) between the bilayer and the substrate which preserves the fluidity exhibited in the membrane native state.[8,52] Locking of a lipid membrane onto the surface is experimentally straightforward in comparison to challenges for producing freestanding bilayer systems. In addition, confined lipid bilayers offer robust and stable platforms that are easy to characterize with a variety of surface-sensitive techniques including quartz crystal microbalance,[53] atomic force microscopy (AFM),[54] and time-of-flight secondary ion mass spectrometry.[55]

**ADVANCED
SCIENCE NEWS**
www.advancedsciencenews.com

**ADVANCED
FUNCTIONAL
MATERIALS**
www.afm-journal.de

Figure 1. Schematic representation (not to scale) of a supported lipid bilayer. Note the presence of a thin water layer between the substrate and the lipid bilayer. Reproduced with permission.[9] Copyright 2006, Elsevier Ltd.

SLBs can be prepared with different techniques[10]: the Langmuir–Blodgett/Langmuir–Schaefer method in which lipid molecules are spread at the air/water interface and then transferred onto the substrate,[8,56,57] or the adsorption and fusion of lipid vesicles to the substrate,[58–60] or the combination of these two methods.[61] A comprehensive review on the advantages and disadvantages of different SLB preparation methods can be found in refs. [9,10].

There are several applications where SLBs attract interest. They provide a model membrane platform to study the biological processes of plasma membranes such as protein–lipid interactions, protein–protein interactions, and cell adhesion and signaling.[43,62–65] SLBs can be also exploited to realize biological and chemical sensors and on-chip immunoassays in combination with patterning techniques and integrated microfluidic devices.[9,66–68] Recently, SLB-assisted self-assembly of DNA origami was reported, suggesting a new utilization of the SLB as a template for directed self-assembly.[69]

One of the main limitations of SLBs is that membrane proteins cannot retain 100% of their functionality when reconstituted within the SLBs.[62] To address this problem, advanced SLBs such as tethered-SLBs have been developed where the proximal leaflet of the lipid bilayer is grafted to the substrate.[70] Polymer-cushioned lipid bilayers are an example of tethered-SLBs where a polymer layer is covalently linked to the substrate and the lipid bilayer is deposited onto the polymer cushion layer. The presence of such polymer layer decouples the lipid bilayer and the substrate, thus shielding the membrane proteins from the substrate and preserving their functionality.[44,62,70] Since their first discovery, SLBs have been extensively studied and still are an active research field thanks,

particularly, to a strong synergy between nanotechnology and nanofabrication.

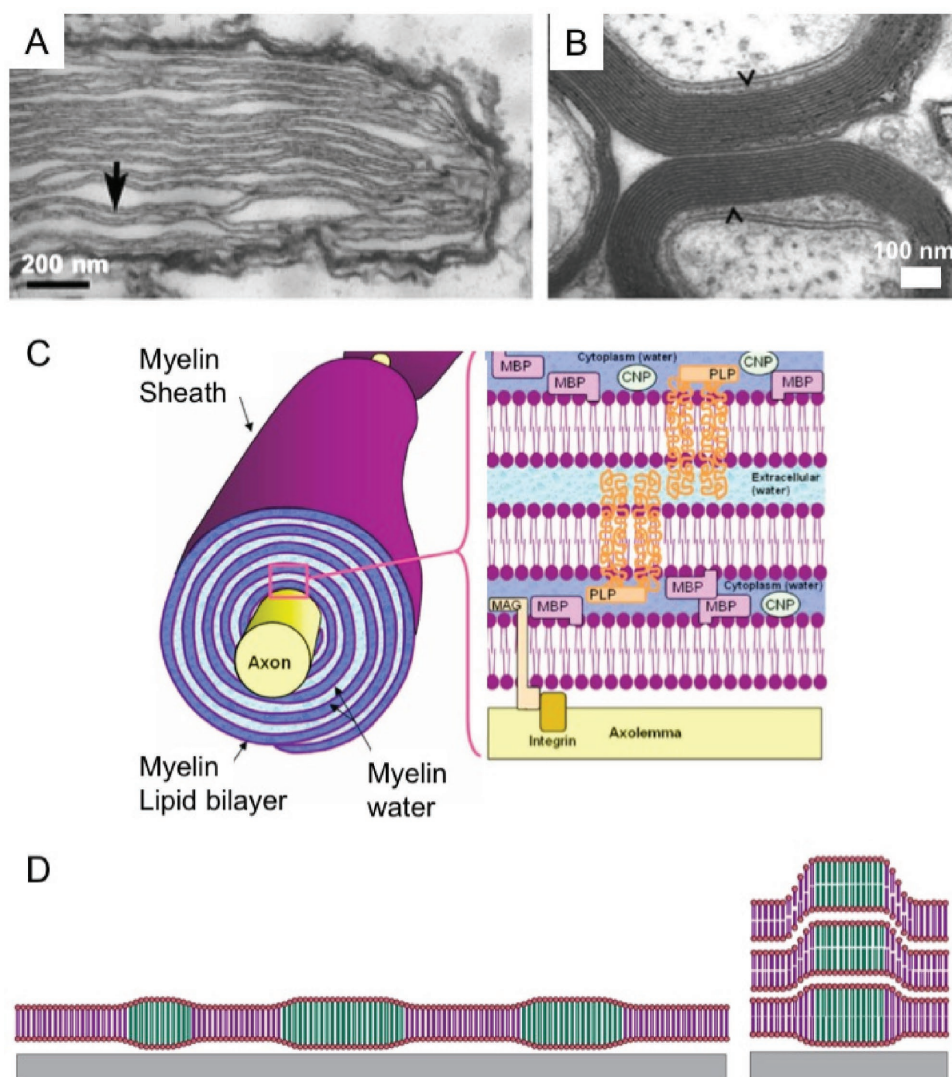## 2.2. Lipid Multilamellar Films

Lipid multilamellar films consist of tens to thousands of lipid bilayers on solid substrates. The extra layers with respect to a supported lipid bilayer add interesting properties and inevitable complexity. The structure of lipid multilamellar films has been thoroughly investigated by means of several techniques including X-ray and neutron scattering/reflectivity and AFM.[46,47,71,72] The structure of lipid multilayers as a function of hydration, temperature, and electric field has also been studied in the context of structural stability.[73–77] Despite substantial research on their structures, applications of the lipid multilamellar films have remained conceptual until recently. Over the past 5 years, the rapid emergence of macroscale delivery systems that require a supported film coupled with the developments of new lipid film preparation methods has spurred the integration of this novel technology into various applications. In this section, we will review recent advances on lipid multilamellar film research, with an emphasis on new methodologies to form lipid multilayers and recently reported applications.

2.2.1. Lipid Supported Bilayer Versus Lipid Multilamellar Films

Lipid multilamellar films provide benefits stemming from the "multilayer" architecture that differentiate their applications from those of SLB. First, lipid multilamellar films can provide a practical platform to mimic the *stacked* membranes found in nature.[79,83–86] Although plasma membranes consist of a bilayer structure, several biological membranes are composed of stacks of bilayer membranes. Examples include thylakoids in the chloroplast of plant cells[83,84] (**Figure 2**A) and myelin sheath in nerves (Figure 2B).[85,86] Figure 2C illustrates multilayered myelin sheaths wrapping around nerve axons. The stacked membranes in such organelles are thought to play an important role in mediating functionality and adaptability to external conditions in those organelles.[87,88] In this regard, lipid multilamellar films can be utilized as model systems to study the structures and functions of certain organelles.

Second, membrane multilayers increase the capacity to store molecules of interest with potential applications in small molecule (drug, genes, and proteins) delivery or sensing. Furthermore, multilayers open the prospect for concurrent delivery of multiple therapeutic agents either sequentially or in a new way mediated by the substrate.[42]

Additionally, recent findings by Tayebi et al.[81] show interesting structural characteristics that lipid multilamellar films can offer, opening up new possibilities of their applications in photonics and sensing. The authors prepared supported lipid lamellar films from the mixtures of sphingomyelin, cholesterol, and unsaturated phospholipids. Phase separation occurred from the multicomponent mixtures, giving rise to liquid-ordered (Lo) domains and liquid-disordered (Ld) domains *in plane*.[81] Interestingly, those phase-separated domains *in plane* aligned themselves across hundreds of bilayers (along the *out-of-plane*

**ADVANCED
SCIENCE NEWS**
www.advancedsciencenews.com

**ADVANCED
FUNCTIONAL
MATERIALS**
www.afm-journal.de

Figure 2. A) Transmission electron microcopy (TEM) of thylakoid membrane stacks found in *Nematodinium* sp. Thylakoids are marked by the arrow. Reproduced with permission.[78] Copyright 2015, Macmillan Publishers Ltd. B) TEM of myelinated axons in rat optic nerve indicated by arrows. Reproduced with permission.[79] Copyright 2015, Association for Research in Vision and Ophthalmology. C) An illustration of multilayered myelin sheaths wrapping around nerve axons. Reproduced with permission.[80] Copyright 2007, Springer New York. D) An illustration of supported model lipid membranes studied by Tayebi et al.[81] Multicomponent lipid bilayers phase separate into coexisting domains (left) and domains align across layers showing interlayer alignment (right). Reproduced with permission.[82] Copyright 2012, Macmillan Publishers Ltd.

direction).[81] Figure 2D illustrates the stacked lipid multilayers with interlayer smectic ordering of the phase-separated intralayer domains. Two features of such domains are particularly interesting—serial coupling and compartmentalization—which may lead to unprecedented membrane functions. For example, transport process and/or electrical signals could be amplified through cooperative behavior of the membrane components dictated by the columnar ordering of phase-separated domains.[81,82]

2.2.2. Advances in Preparation of Lipid Multilayers with Functionality

Several factors act as a bottleneck for the use of lipid multilamellar films in practical applications. The most significant factor is the mechanical and chemical instability of the lipid films. Multilamellar lipid films often cannot withstand the perturbation induced by the buffer solution (delamination and disruption upon hydration)[73] and they are susceptible to oxidation (especially in the case of unsaturated lipids).[89,90] Also, the addition of functional components to the lipid films often provides the challenge of retaining the functionalities of those components during the integration process (e.g., drying of lipid amphiphiles in an organic solution is a simple way to form self-assembled lamellar films but the membrane proteins cannot retain their biological activity while going through such a process).[91] For practical applications, it is important to develop methods to incorporate functional components in the lipid films without losing the structure and functionality of the lipid assemblies. In addition, to serve as model membranes,

the existing lipid multilamellar films should be further developed to better mimic the complexity of nature's membranes. To this end, new approaches to prepare lipid films have been suggested. In this subsection, we will introduce some of the new methods to prepare lipid lamellar films, highlighting their significance in relation to potential applications.

Overall, the preparation of lipid multilamellar films can be divided into two different approaches. One is bulk-scale direct spreading and the other is a layer-by-layer (LBL) assembly approach. The direct spreading consists of depositing stock solutions of lipids dissolved in an organic solvent to the substrates either by drop casting or spin coating.[92] By controlling the spin-coating conditions or the density of stock solutions, one can control the thickness of the stacked bilayers. This procedure rapidly yields multilamellar lipid films even on a large scale.

Based on the direct spreading method, Gupta et al.[93] introduced a way to construct lipid-based multilamellar films with improved structural integrity. The authors have prepared composite lipid–silica films by spin-coating lipids onto a substrate first and then exposing the lipid film to vapors of a silica precursor, tetraethyl orthosilicate, as schematically shown in **Figure 3**A. During the chemical vapor deposition (CVD) process, silica molecules are assumed to penetrate the lipid bilayer stacks and to condense in the water layer within the lipid bilayers, supposedly interacting with lipid hydrophilic headgroups. The final structure of the lipid–silica composite films comprises alternating lipid bilayers and silica–water layers, maintaining long-range alignment of stacked lipid bilayers. The lipid–silica composite films were robust in air for at least 6 months and stable in aqueous solutions (no delamination was observed). More importantly, the fluidity of lipid membranes was retained in the presence of silica, which is important for mimicking biologically relevant conditions. These lipid–silica composite films may serve as robust model systems to study the fundamental properties of stacked membranes and as durable platforms for device integration. Although composite lipid films have been less explored, they could potentially provide new solutions to overcome the weak stability of lipid films while preserving native properties of lipid membranes. In this regard, composite lipid–polymer hybrid films are reviewed in Section 3.

The LBL method yields multilayered lipid films by depositing bilayers one by one. A commonly used method to form a base bilayer in contact with the substrate is to induce rupture of giant unilamellar vesicles (GUVs) or large unilamellar vesicles (LUVs) at the substrate surface. To add subsequent bilayers a variety of different mechanisms have been explored, including electrostatic attraction, complementary functional group interactions (e.g., biotin–streptavidin coupling,[96] DNA hybridization[97]), or specific surface chemical interactions (e.g., maleimide–thiol coupling,[64] N-hydroxysuccinimide/1-ethyl-3-(3-dimethylaminopropyl)-carbodiimide,[98] and amine-sulfhydryl crosslinking[99]).

Heath et al.[94] applied the traditional LBL method in which subsequent layering occurs via electrostatic interactions. The negatively charged lipid bilayer (1-palmitoyl-2-oleoyl-sn-glycero-3-phosphocholine or POPC/1-palmitoyl-2-oleoyl-sn-glycero-3-phospho-(1′-rac-glycerol)) was formed via vesicle rupture and positively charged poly-L-lysine (PLL) was deposited between lipid bilayers acting as an electrostatic polymeric glue (schematic illustration in Figure 3B). This approach allows to accommodate a range of proteins in separate bilayers by rupturing different types of proteoliposomes in each bilayer deposition
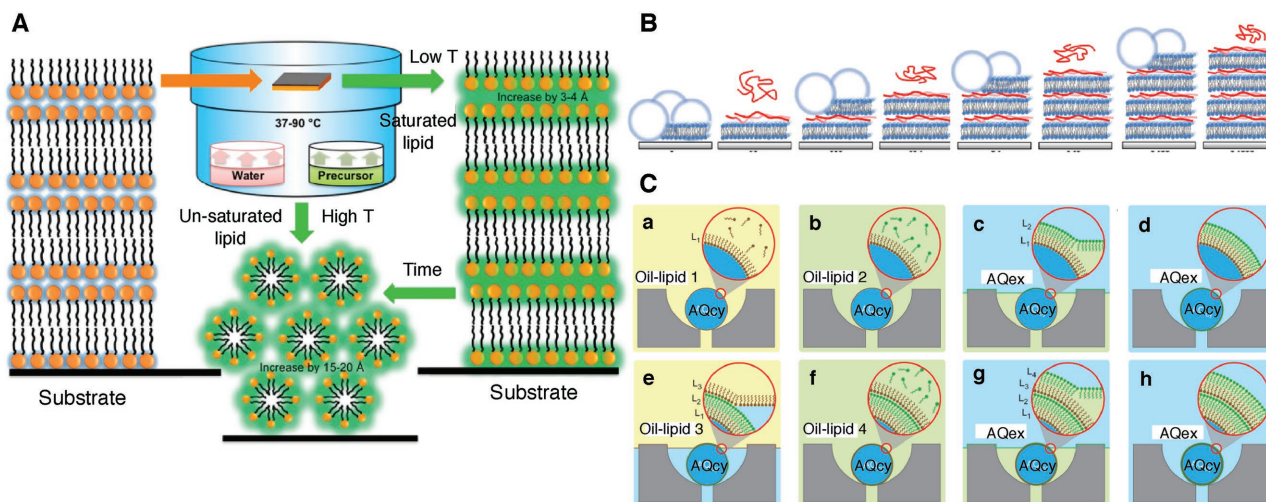
Figure 3. A) Schematic illustration of the CVD process that produces silica encapsulated multilamellar lipid films. When lipids films are exposed to a silica precursor/water vapor environment, silica locate between lipid bilayers (represented in green). Reproduced with permission.[93] Copyright 2013, American Chemical Society. B) Schematic of the buildup process of multilamellar lipid-poly L-lysine films. The lipid vesicle is ruptured and fused onto the substrate followed by addition of PLL (red ribbon) to the lipid bilayer. The steps are repeated to form additional bilayers. Reproduced with permission.[94] Copyright 2015, American Chemical Society. C) Schematic of LBL assembly on microfluidic droplets that enables to build membranes with *transbilayer asymmetry*. a) Water-in-oil droplets are trapped in a capture cup. c,e,g) Each phase-boundary crossing over the immobilized droplets deposits a new monolayer of lipids on the droplets. Changing the lipid composition in the steps (b) and (f) enables to build asymmetric transbilayers. AQcy stands for aqueous cytoplasmic material and AQex denotes extracellular aqueous phase. Reproduced with permission.[95] Copyright 2012, Macmillan Publishers Ltd.

**ADVANCED
SCIENCE NEWS**
www.advancedsciencenews.com

**ADVANCED
FUNCTIONAL
MATERIALS**
www.afm-journal.de

step. In addition, the LBL process utilizing electrostatic interactions is less time consuming and less costly compared to processes that leverage direct chemical interactions.

A novel LBL procedure devised by Matosevic and Paegel allows to build multilamellar lipid membranes with programmable lamellarity (the number of lipid bilayers) and transbilayer asymmetry (bilayers in which each layer has a different composition).[95] As illustrated in Figure 3C, such layering procedure[95] makes use of monodisperse lipid-stabilized water-in-oil emulsions that are entrapped on microfluidic droplet arrays. The strategy is to mobilize the oil/water phase boundaries over stationary droplets instead of making droplets cross the stationary phase boundaries. For each deposition step, a lipid *monolayer* is formed on the immobilized droplets crossing the oil/water phase boundary. Because the deposition unit is a *monolayer*, this method allows to build asymmetric lipid bilayers by varying the chemical composition of the oil-lipid phase. This work provides a systemic route to make model membranes that closely mimic natural cell membranes where the transbilayer asymmetry is ubiquitous.

Recent advances in lipid film preparation which are mentioned above hold promise for developing systems that are capable of confining or compartmentalizing molecules of interest. Not only limited to model membrane systems, such functionality of lipid films could be further applied to engineer advanced drug delivery systems to codelivery of multiple types of drugs in sequential steps.

In addition to the aforementioned methods other approaches have been developed. Electrospraying has been employed to coat complex porous surfaces, such as those encountered in food products and pharmaceuticals, with lipid thin films.[100] Patterning or stamping of stacked lipid bilayers was achieved by polymer stencil lift-off[101] or dip-pen nanolithography[102] for applications in drug screening and sensing. Building of lipid multilayers from an aqueous dispersion[103] was also attempted to facilitate the inclusion of hydrophilic molecules into the lipid films.

2.2.3. Recent Applications of Lipid Multilamellar Films

Early application studies on lipid multilamellar films have focused on the structural properties of reconstituted transmembrane proteins. Recent applications on multilamellar films, however, show that lipid layers supported on a substrate can also have a wide variety of uses. Those applications include artificial cell substrates,[64] bioelectrocatalytic systems for biosensors or photovoltaic cells,[104] matrixes for macroscale drug delivery devices,[105] and substrate-mediated gene delivery.[106] More generally, the use of lipid films to direct the assembly of functional soft and hard materials has been suggested.[107]

Advances on lipid multilamellar films have been driven by the capability of the lipid films to mimic complex multilamellar membranous structures found in nature. A noteworthy direction in lipid film research is their application as a supported film platform for biomaterial-based implantable electronic/photonic devices to realize remotely controlled therapy,[105] which is a rapidly growing field. **Figure 4** summarizes recent research directions toward practical applications of lipid multilamellar films.

Artificial Cell Substrates: The extracellular matrix (ECM) provides the physical and biochemical support for surrounding cells. Lipid multilamellar films have been exploited as a cell substrate mimicking the native environment of the ECM.[64,99] Cell behavior on polymer-tethered lipid multilamellar films was studied in response to the viscoelastic properties of the films (Figure 4A).[99] The viscoelastic properties of the cell substrates could be tailored by controlling the number of lipid bilayers or the density of cell adhesion ligands incorporated in the top layer.

Bioelectrocatalytic Systems: In nature, electron transport mediated by quinones commonly takes place in the mitochondrial cristae or in the thylakoid stacks in chloroplasts. Quinones are coenzymes that shuttle electrons between membrane enzymes, leading to energy transduction or storage. Heath et al.[104] recently constructed a lipid multilayer matrix with redox-active membrane enzymes for the purpose of mimicking the function of mitochondrial cristae and thylakoid stacks (Figure 4B). Several lipid–protein bilayers were assembled onto gold electrodes using the LBL method. Lipid membranes containing quinones and quinone-converting enzymes successfully provided electron transfer across the membrane layers, as confirmed by means of cyclic voltammetry. Quinones were suggested to diffuse through defect sites within the lipid films where neighboring lipid bilayers are interconnected. We believe that this pioneering work will stimulate future studies that model protein interactions in stacked lipid membranes, and advance this field, a step closer to mimic the inherent membrane complexity observed in nature.

Macroscale Drug Delivery: Macroscale drug delivery (MDD) device, a term defined by Kearney and Mooney,[41] refers to a system delivering bioactive agents such as genes, drugs, and proteins to the desired site by implantation or injection. In order to exert spatiotemporal control over drug storage and release, macroscale biomaterials are often combined into MDD devices in the form of a matrix or reservoir. Hydrogels and polymers have been extensively explored as candidate macroscale biomaterials,[108–110] but in comparison there is a shortage of MDD studies that leverage lipids as the carrier material. Our group recently reported temperature-sensitive lipid multilamellar films that are integrated with electronically programmable and frequency-multiplexed wireless hardware (MDD device).[105] Multiple types of drugs were incorporated into the lipid membranes where the drug transport was actuated by the temperature-induced phase transitions of the lipid films (Figure 4C). Below 40 °C, the lipid multilayers comprised two coexisting phases: liquid ordered and liquid disordered. Upon an increase in temperature, the Lo phase transformed into the Ld phase, facilitating diffusion of the hydrophilic drugs out of the films. The thermotropic phase transition of lipid films is a useful handle that could be used to switch "on/off" implantable drug delivery systems.

Substrate-Mediated Gene Delivery: Lipid films also play a role as gene delivery matrices that incorporate genes and deliver them at localized sites (Figure 4D). The delivery of genes from surfaces is also referred as substrate-mediated or surface-based gene delivery. Substrate-mediated gene delivery holds tremendous potential in many biomedical research applications, including medical implant coatings,[111] inductive tissue engineering,[112] and transfected cell microarrays for high-throughput genomic studies.[113,114] To date, carrier materials
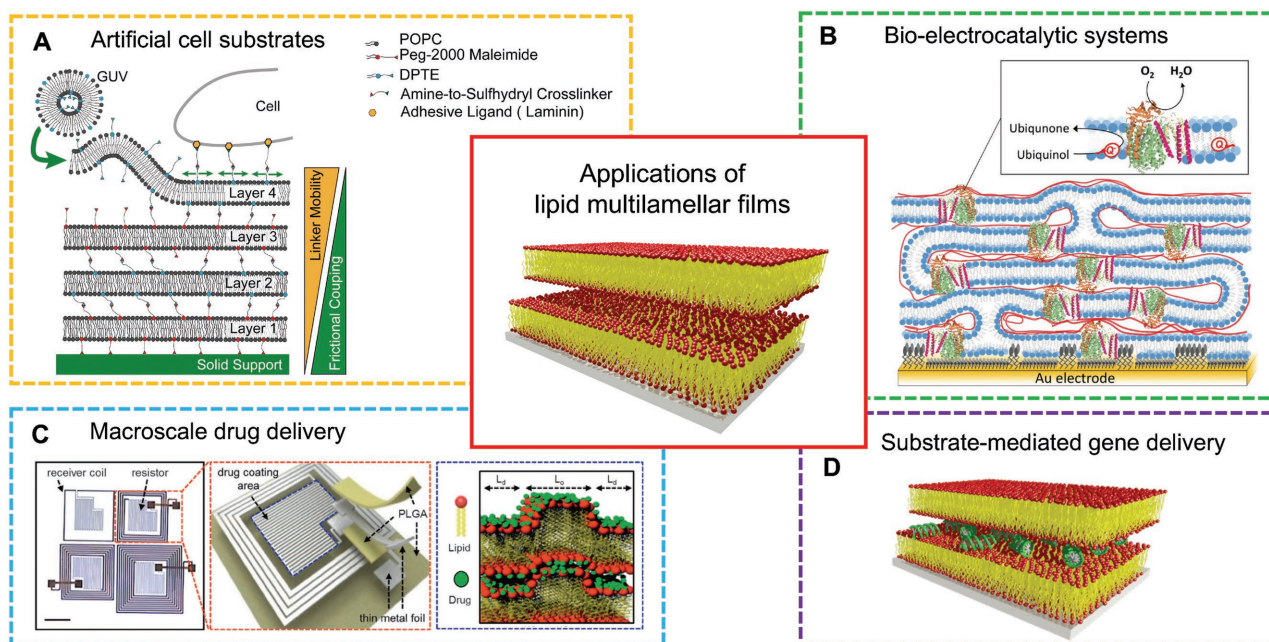
Figure 4. Applications of lipid multilamellar films. A) Artificial cell substrates. DPTE stands for 1,2-dipalmitoyl-*sn*-glycero-3-phosphothioethanol. Reproduced with permission.[99] Copyright 2013, Elsevier Ltd. B) Bio-electrocatalytic systems. PLGA stands for poly(lactic-*co*-glycolic acid). Reproduced with permission.[104] Copyright 2017, WILEY-VCH. C) Macroscale drug delivery. Reproduced with permission.[105] Copyright 2015, Macmillan Publishers Ltd. D) Substrate-mediated gene delivery.

used in substrate-mediated drug/gene delivery are largely polymers[42] and the use of lipid films as the matrix is scarce. We will point out important aspects for utilizing lipid films in substrate-mediated gene delivery in this section. Our contributions in substrate-mediated siRNA (small or short interfering RNA) delivery are discussed in Section 2.3.

Lipid-DNA films have been successfully reported in several studies.[115–117] During the film preparation process, DNA molecules are intercalated between lipid bilayers. Interestingly, it was shown that DNA undergoes a reversible phase transition between double stranded (active) and single stranded (nonactive) conformations under wet and dry conditions, respectively. Concomitant structure changes of lipid (dimethyldidodecylammonium bromide) layers were observed between bilayer and single layer under wet and dry conditions, respectively. Such phase transition confers greater gene storage capabilities of lipid-DNA films with humidity-responsive properties, which would be advantageous in MDD applications.

Recent studies by Perry et al.[106] tested the in vitro DNA transfection efficacy of lipid-DNA films (transfection is the process of deliberately introducing genetic materials into mammalian cells). The reported transfection level was very low for the solid films compared to their analogs in particulate form. Although the gene delivery mechanism from the lipid-DNA films should be further explored, it is postulated that film disassembly plays a significant role in determining the cellular uptake of DNA. Despite this challenge and the low transfection efficiency, lipid-DNA films are still promising gene delivery materials because lipid molecules can be tuned to quickly respond to external stimuli. In this regard, future studies in lipid-film-mediated gene delivery should be geared toward understanding cellular uptake mechanisms of genes at a fun-

damental level with the goal to achieve high DNA transfection efficacies. We will further discuss the responsive behavior of lipid films and their associated applications in Section 2.3.
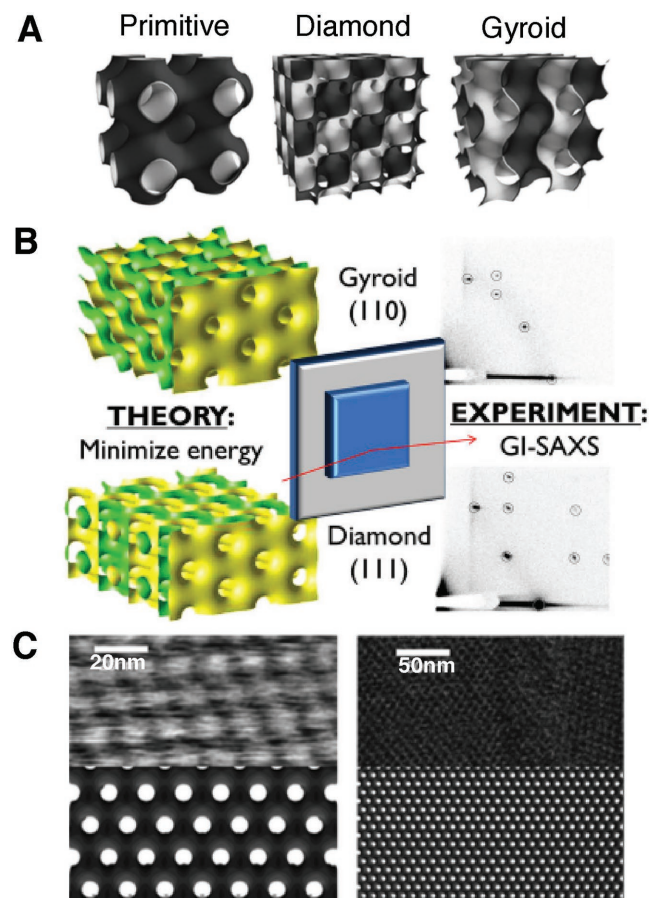
2.3. Nonlamellar Lipid Films

Of the two main characteristics of lipids, i.e., excellent biocompatibility and polymorphism, the former has been the main driver for using lipid films into various systems such as implantable medical devices or cell membrane mimicking structures. The latter, however, has gained considerably less attention in the field of lipid film research. In light of the importance of lipid polymorphism in bulk (hereafter used to refer to bulk gels or suspensions), the lipid phase behavior, when confined to a surface, is also expected to play an important role for promoting the applications of lipid films. However, to enable such applications, the structure and properties of nonlamellar lipid films should be better understood. In this section, we will describe the current understanding of lipid polymorphism on confined surfaces, highlighting the applications enabled by their unique capabilities.

2.3.1. Lipid Phase Behavior on Surfaces

In general, the phase diagram of lipids obtained for bulk systems are translated into films (although there are slight changes that will be discussed later). One can attain nonlamellar phases of lipid films using the same composition and temperature that yield to bulk systems. This includes inverted hexagonal phases (H_{II}),[16,24] inverse discrete micellar cubic (Q^{227}, *Fd3m*),[23,24] and

**ADVANCED
SCIENCE NEWS**

www.advancedsciencenews.com

**ADVANCED
FUNCTIONAL
MATERIALS**

www.afm-journal.de

inverse bicontinuous cubic (Q_{II}) phases of two distinct symmetries (diamond $Pn3m$ and gyroid $Ia3d$).[16,25,118,119]

In the category of "nonlamellar" films, the preparation of lipid bicontinuous cubic phase films is of particular interest. These structures comprise a continuous lipid bilayer where the mid-planes (the middle of the bilayer) conform to periodic minimal surface with the negative Gaussian curvature. The bilayer is in contact with two interwoven yet unconnected networks of water channels (**Figure 5**A).[118,120] Such inherent structure of the lipid cubic phase yields large surface area to volume ratios with uniform water channels and 3D isotropic diffusion.[14] Bicontinuous lipid cubic phases in bulk have been utilized for various applications including membrane protein crystallization and drug/gene delivery.[14,17,121–123]

Monoolein (MO) and phytantriol molecules, well known from the cubic phase in bulk, also form cubic phases in supported thin films.[25,119] We recently prepared a positively charged gyroid phase (Q_{II}^G) to incorporate negatively charged siRNA in the lipid films, by including a cationic lipid, 1,2-dioleoyl-3-trimethylammonium-propane (DOTAP) to the MO mixtures.[16] Unlike lipid multilamellar films, the lipid cubic phase films can be prepared exclusively by drop casting or spin coating from organic solutions including lipids.

The structure of the lipid cubic phase films has been mainly investigated by grazing-incidence X-ray scattering (GISAXS) and AFM. GISAXS in reflection geometry provides structural information in both parallel and perpendicular directions to the thin film surface. Averaged information on the lipid cubic phase films regarding the symmetry (space group), unit cell size, and alignment on surfaces can be readily obtained from the GISAXS measurements. Figure 5B shows an example of GISAXS data obtained for the lipid bicontinuous cubic diamond phase with the (111) plane and gyroid phase with the (110) plane oriented parallel to the substrate.[119] While time-resolved synchrotron experiments would enable the investigation of phase transition kinetics, GISAXS as an average technique cannot provide information on the boundary region between adjacent domains or on the interfaces between the films and air or water. In this regard, AFM measurements can provide complementary information on the structure of the lipid films because AFM allows direct visualization of domain size, individual water channels, and epitaxy in the lipid films.[118] Figure 5C presents AFM images of supported Q_{II} phases in excess water where the nanostructure and film epitaxy is clearly seen.[118]

From the characterization of the lipid cubic phase films, one prominent feature was observed. Lipids align themselves in a highly ordered manner exhibiting preferential orientation with respect to the substrate. This process is driven by the interfacial energy between the lipid phase and the substrate. When the lipid bilayers of the cubic phase are in contact with the surface, they form a closed structure such that the lipid bilayer's free edges are shielded due its hydrophobicity. The closure of the bilayers in the cubic periodic structure results in the formation of both positive and negative mean curvatures, which generates the energy cost to bend lipid bilayers (called bending energy).[119,124] Thus, when the lipid cubic phase encounters the substrate interface, it aligns with respect to the substrate in a way that minimize the interfacial energy.[119,124] The preferential orientation adopted by the cubic phase films can be predicted from thermodynamic interfacial energy calculations and is well corroborated by experimental observations.[119] Those oriented films could provide a good model system to study the pathways of lipid phase transitions, unveiling the epitaxial relationships during transformations.[125–127]

Nylander et al.[24] recently investigated the layers *dynamics* in the cubic ($Fd3m$) phase and hexagonal (H_{II}) phase at an Si substrate surface. The cubic phase layers appeared more rigid at the substrate interface compared to the hexagonal phase layers based on neutron reflectometry and grazing incidence neutron spin echo spectroscopy experiments. The rigidity of the $Fd3m$ phase is attributed to the suppressed undulations at the interface whereas the H_{II} phase experiences undulations coming from the hydrodynamic interactions between the H_{II} phase

Figure 5. A) Schematic representation of three different bicontinuous cubic phases. The minimal surface represents the mid-plane of a lipid bilayer. Each side of the bilayer has a water domain (represented in dark grey and white) and these domains do not penetrate. Reproduced with permission.[118] Copyright 2010, The Royal Society of Chemistry. B) The crystallographic orientation that cubic phase film adopts with respect to the surface can be predicted from theoretical considerations of surface energy minimization. The predictions are in good agreement with experimental observation. Reproduced with permission.[119] Copyright 2014, American Chemical Society. C) AFM images of the diamond cubic phase in water (top) and simulated surface of (111) plane of the cubic diamond phase. The cubic phase films can be directly imaged using AFM. Reproduced with permission.[118] Copyright 2010, The Royal Society of Chemistry.

cylinders and the substrate. It is notable that the distance from the substrate to the first H_{II} layer seemed to affect the length of the hexagonally ordered cylinders with their long axis parallel to the surface. Further studies on the effect of the surface could provide a valuable design handle for controlling the domain size of lipid H_{II} phase films.

Limited work has been carried out to study the effect of different substrates on the cubic structure and its dynamics in nonlamellar lipid films. It would be interesting to understand the role of hydrophilic/hydrophobic functionalization of the surface in determining the structure of the lipid nonlamellar phase on solid supports (e.g., the domain alignment, flexibility of the layers, and shift in phase boundaries). Understanding the self-assembly, thermodynamics, and dynamics of lipid films onto solid supports will allow for their rational design of functional films with tunable polymorphic properties.

2.3.2. Applications of Nonlamellar Lipid Films

Applications of nonlamellar lipid films are almost unexplored at this point. Nanostructured lipid thin films have been utilized as matrices for substrate-mediated gene delivery,[16] as templates for in situ metal growth into periodic nanostructures,[128,129] and as host materials to incorporate nanoparticles with macroscopic alignment.[107] Since we limit the scope of this paper to biomedical-related applications, here we only discuss the applications of nonlamellar lipid films to substrate-mediated gene delivery.

We have recently prepared three different lipid films adopting a 1D lamellar, 2D H_{II} and 3D Q_{II}^G or mixture of two phases with proper control of lipid compositions, temperature, and relative air humidity.[16] Those lipid films were shown to experience reversible phase transitions from one to another phase upon a temperature or humidity change.

When siRNA molecules were incorporated into the lipid films via electrostatic interactions, we observed slight changes in the phase behavior (**Table 1**) compared to neat lipid films.

Such effect of siRNA incorporation on the lipid phase has been observed for bulk systems too.[130] Also, note from Table 1 that the lipid-siRNA films exhibit shifted phase boundaries compared to the lipid-siRNA particulates in solution. For example, the Q_{II}^G and H_{II} phases are preserved at higher DOTAP molar percent in films compared to bulk possibly because of different interactions between films and bulk with respect to the introduction of siRNA negative charges to the assemblies. The lipid films are interfaced with two parts—the substrate and water layer—whereas the particulates are only exposed to bulk water. The changes in the net charge of the lipid headgroups due to siRNA pinning affect the effective area per lipid headgroup and hence the lipid molecule geometry. In turn, this concomitantly alters the interfacial energy, which is a function of the mean curvature of the membranes in the lipid constructs. Such changes in interfacial energy accompanied by membrane charge density overall may affect the epitaxial (orientational) relationships during phase transformations (Q_{II}^G to H_{II} and H_{II} to L_α), resulting in the shifts of the phase boundaries.

Figure 6 shows GISAXS diffraction patterns of a Q_{II}^G phase before and after siRNA incorporation. The elongated diffusion spots after siRNA inclusion indicates that some degree of order is lost with a distribution of domain orientations, but the preferred uniaxial orientation is still preserved. We observed uniaxial orientation of the lipid-siRNA film for the whole film thickness ($\approx$30 µm). Previous study reported the case in which the composite lipid films conditionally show out-of-plane alignment with respect to the substrate.[129] We expect further studies would disclose the relationship between the film thickness and the structure alignment in terms of interfacial energy.

When three different nanostructured lipid films were applied in siRNA knockdown experiments, the Q_{II}^G phase film showed the superior siRNA silencing efficacy compared to other films. This is attributed to the inherent structural properties of the Q_{II}^G phases that possess positive Gaussian elastic modulus leading to efficient endosomal escape.[16,17] The significance
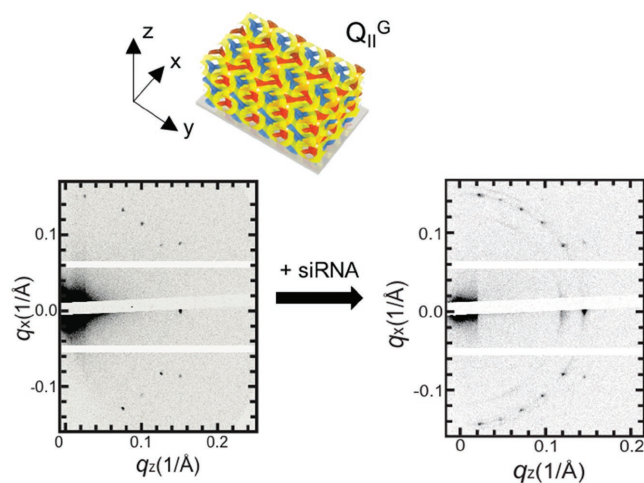
Table 1. Phase diagram of MO/DOTAP lipid films with and without siRNA. RH stands for relative air humidity. Q_{II}^G, H_{II}, and L_α symbols represent a bicontinuous gyroid cubic, an inverted hexagonal, and a lamellar phase, respectively. Reproduced with permission.[16] Copyright 2016, WILEY-VCH.

Molar fraction of DOTAP in MO/DOTAP films	Dry film (25 °C, 20–40% RH)		Wet film (37 °C, (95 ± 5)% RH)		Bulk solution (37 °C)	
	−siRNA	+siRNA	−siRNA	+siRNA	−siRNA	+siRNA
0.15	L_α	L_α	Q_{II}^G	Q_{II}^G	Q_{II}^G	Q_{II}^G
0.25	L_α/H_{II}	L_α/H_{II}	Q_{II}^G	Q_{II}^G	Q_{II}^G	Q_{II}^G
0.3	H_{II}	H_{II}	Q_{II}^G	$Q_{II}^G + H_{II}$	Q_{II}^G	H_{II}
0.4	H_{II}	H_{II}	Q_{II}^G	$Q_{II}^G + H_{II}$	Q_{II}^G	$H_{II}+L_\alpha$
0.5	H_{II}	H_{II}	L_α	L_α	L_α	L_α
0.75	H_{II}	H_{II}	L_α	L_α	L_α	L_α

Figure 6. GISAXS data of MO/DOTAP films (molar fraction of DOTAP = 0.3) before and after siRNA incorporation equilibrated at air humidity. Upon siRNA addition, the Q_{II}^G phase transformed into a mixture of the Q_{II}^G and H_{II} phases. Note that lipid-siRNA films are more disordered compared to the lipid-only films. Reproduced with permission.[16] Copyright 2016, WILEY-VCH.

of this work is the exploitation of nanostructures for the first time to regulate the efficacy in substrate-mediated gene delivery applications. Also, it is worth noting that the responsive phase behavior of nanostructured lipid thin films was controlled with changes in relative humidity. Lipid assemblies, especially liposomes, have received tremendous attention as *stimuli-responsive* materials in various fields. They can be prepared to be responsive to external stimuli such as water content, temperature, pressure, or ultrasound,[20] mimicking the responsiveness of living organisms. Different lipid phases show distinct properties of molecular diffusion, cell adhesion, and permeation, etc.[14,16,121,131] Thus, the use of lipid nanostructured films that take advantage of stimuli-responsive properties could give rise to tunable diffusion and adhesion/permeation properties for encapsulated molecules of interest.

On a final note, recent studies of lipid cubic phases in bulk are widening their functionality, which could further extend future applications of lipid cubic phase films. For example, Mezzenga and co-workers demonstrated that lipid cubic phases in bulk can serve as matrices for the detection of a vast class of analytes including disease biomarkers, viruses, bacteria, and parasites, based on the optical properties of the bicontinuous cubic phase.[19] Specifically, the optically isotropic lipid cubic phases become birefringent upon enzymatic reactions which can be monitored via optical detection.[19] These changes in optical properties could be further leveraged in cubic phase thin films for biocatalytic fuel cells that utilize biocatalytic reactions as a fuel to generate electrical power and biosensors that enables high throughput screening.

3. Lipid–Polymer Hybrid Membranes

Block copolymers composed of hydrophilic and hydrophobic groups can self-assemble into various structures in a similar manner to lipids such as micelles, vesicles, and tubes.[132,133] Despite the similarities between lipids and block copolymers in terms of their amphiphilic nature and the ability to self-assemble into various morphologies, research on lipid assemblies and block copolymer assemblies have followed separate routes.

Polymer assemblies and lipid assemblies show different physicochemical properties. Polymersome membranes are usually thicker (≈8–50 nm per single bilayer) than those of liposomes (≈5 nm per single bilayer) because of the higher molecular weight of the polymer blocks. The thicker polymer membranes provide better stability and higher mechanical strength compared to liposomes[48,49,134,135] but also yield poor membrane permeability, limiting the diffusion of small molecules encapsulated inside polymersomes,[134] and poor membrane-fusion capabilities. The breadth of block copolymer's synthetic routes allows versatility to modulate chemical functionality but simultaneously results in lack of biocompatibility. In contrast, lipid membranes found in all cell membranes are biocompatible.[48,49]

In an effort to combine the benefits of the two materials, hybrid systems, composed of lipid–polymer mixtures, have been recently explored.[136–138,49,139–141] By mixing lipids and block copolymers in the same membrane, one can expect to obtain hybrid membranes with tunable structural properties and good biocompatibility. A broader range of chemical compositions, molecular weight, hydrophobicity, and surface charge of assembling building blocks (i.e., block copolymer and lipids) enables modulation of the hybrid membranes physicochemical properties including permeability, mechanical stability, and solubility of encapsulated molecules. Moreover, from a materials science perspective, hybrid systems of two different materials are exciting as they may give rise to new structures and properties otherwise not attainable with single component systems.
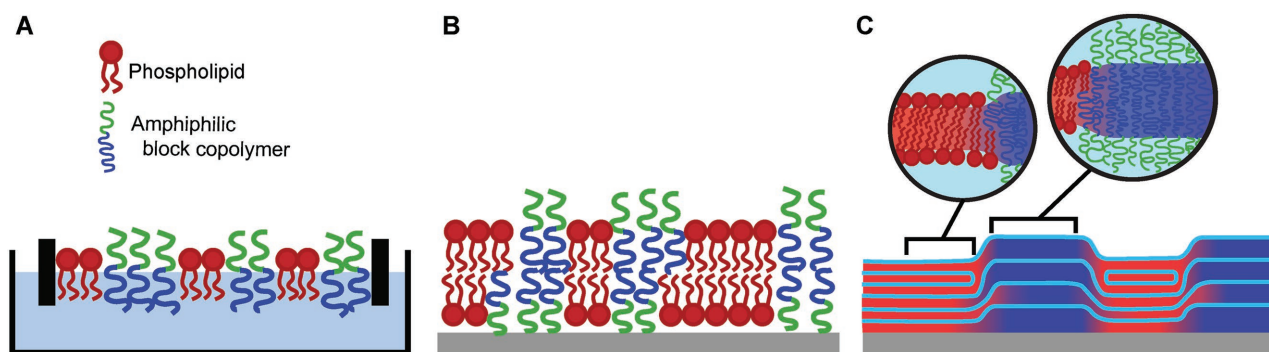
Research on lipid–polymer hybrid membranes is at a very early stage with just a few studies reported so far. However, previous work already alludes to numerous potential applications of hybrid membranes. This includes model systems mimicking plasma membranes, sensors, and small molecule (drug, genes, and proteins) delivery platforms. Hybrid vesicles, composed of mixtures of phospholipids and block copolymers, have been shown to form various membrane phases with different miscibility.[48,139] Molecular and macroscopic parameters such as copolymer architecture, lipid fluidity, hydrophobic mismatch, or chemical compatibility between lipids and polymers determine the phase of the hybrid vesicles. Both lateral phase separation at the nanoscale and micrometer scale and complete fission into separate vesicles have been reported.[48,49] Careful selection of lipid and copolymer molecules with engineering parameters such as temperature, cooling rate, and osmotic control enables the modulation of phase separation at the micro- and nanoscale.[50,140–142] Such complicated but diverse phase behavior of lipid–polymer hybrid systems may offer new insights to understand complex plasma membrane systems where the presence of phase separated domains goes beyond classical liquid-ordered and disordered lipid-only phases. Also, the compositional variety of hybrid membranes could possibly confer advanced functionalities such as control over membrane compartmentalization, diffusion rates of membrane components, and mechanical stability.

The original studies on lipid–polymer hybrid membranes were performed on GUVs because of the ease of optical characterization. Besides GUVs, recent work has explored other systems including LUVs,[142] tubular vesicles,[143] planar membranes,[144,145] and most recently from our group, multilayered films.[146]

In this section, we will review lipid–polymer hybrid systems focusing on planar membranes in the form of suspended monolayers, solid-supported bilayers, or multilayered films on solid supports. **Figure 7** shows the schematic illustration of those three different lipid–polymer hybrid membrane systems. We will highlight the approaches explored to construct hybrid membranes, followed by their structure, function, and possible applications of these newly assembled structures.

3.1. Suspended Lipid–Polymer Monolayer

Mixed lipid–polymer monolayers at the air/water interface have been studied as a platform for directed membrane protein insertion and for controlled localization of polymer-functionalized nanoparticles in the membranes. Two important features of the mixed lipid–polymer monolayer give rise to controlled distribution of molecules embedded into the hydrophobic

ADVANCED
SCIENCE NEWS
www.advancedsciencenews.com

ADVANCED
FUNCTIONAL
MATERIALS
www.afm-journal.de

Figure 7. Schematic illustration of lipid–polymer hybrid membranes with different structures. A) Suspended monolayer in water, B) supported bilayer on solid substrate, and C) multilayered films on solid substrate. Panel (C) reproduced with permission.[146] Copyright 2017, American Chemical Society.

region: surface hydrophobicity and heterogeneity (phase-separated domains).[145,147]

Kowal et al.[145] combined amphiphilic copolymer poly(dimethylsiloxane)-*block*-poly(2-methyl-2-oxazoline) or PDMS-*b*-PMOXA with various phospholipids to investigate and tailor the incorporation of membrane protein into the monolayer. The mixtures of lipids and polymers resulted in phase separation of two components into different domains. The lipid–polymer compositions determined the size and shape of phase-separated domains. Interestingly, membrane proteins were preferentially located into the more *fluid* regions of the monolayer. When saturated lipids (1,2-dipalmitoyl-*sn*-glycero-3-phosphocholine (DPPC), 1,2-dipalmitoyl-*sn*-glycero-3-phosphoethanolamine (DPPE)) were mixed with PDMS-*b*-PMOXA, proteins favored the polymer-rich domains over lipid-rich domains while the opposite trend was observed for unsaturated lipid (DOPC)–polymer mixtures. This work introduces a new possibility to engineer model membranes that are biologically relevant by introducing membrane proteins with controlled distribution at the desired sites.

The work by Olubummo et al.[147] also demonstrates the localization of molecules of interest (polymer-coated nanoparticles) into mixed lipid–polymer monolayers made of poly(isobutylene)-*block*-poly(ethylene oxide) or PIB-*b*-PEO and phospholipid DPPC at the air/water interface. It was observed that the presence of PIB-*b*-PEO in the hybrid layer disturbs the lipid packing, inducing rearrangement of the lipid molecules. In addition, the lipid–polymer system phase separated into different domains with the size of the polymer domains increasing with the polymer content. The surface functionalization of the CdSe nanoparticles played a pivotal role in controlling the location of those nanoparticles in the monolayer. The particles coated with PIB were homogeneously distributed whereas the ones coated with PIB-*b*-PEO showed heterogeneous distribution (preferentially embedded into the polymer domains).

Partitioning molecules into selective membrane regions is an interesting outcome enabled by the mixing of different self-assembling building blocks: lipids and block copolymers. The factors driving phase separation of lipid–polymer mixtures should be further explored to fine control the layer structure and the distribution of molecules of interest. Hybrid monolayer systems may be useful to the development of membranes where the spatial control of the embedded components is required.
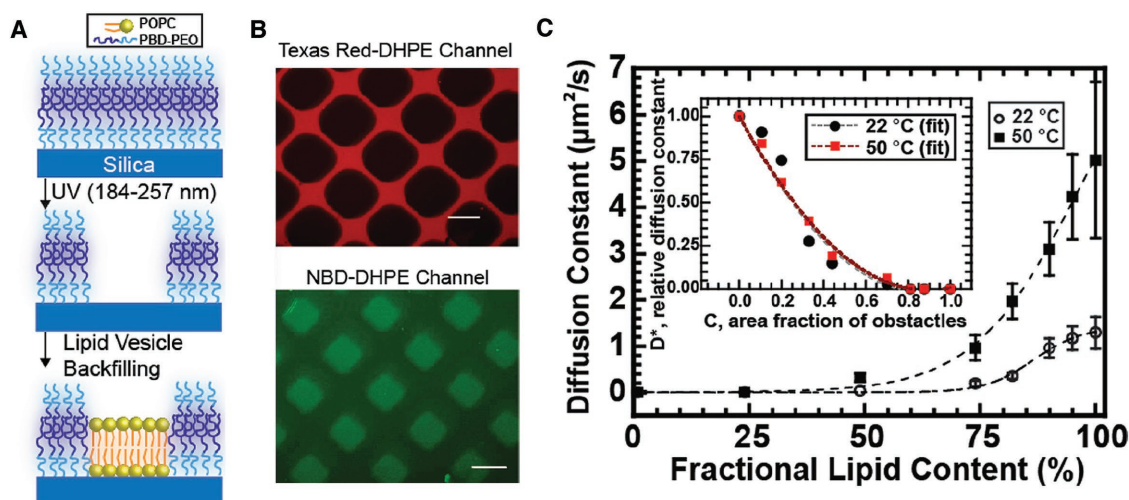
3.2. Supported Lipid–Polymer Bilayer

Supported lipid–polymer bilayers (SLPB) are analogs to supported lipid bilayers but differ in composition as they comprise of block copolymers in addition to lipids. It should be noted that SLPBs differ from polymer cushioned lipid bilayers where a hydrophilic polymer brush is located between a (polymerized) lipid bilayer and the solid support. While polymer brush–SLB systems utilize polymers to fill the space between lipid bilayers and the substrates, polymers in SLPBs interact with the lipids within the same bilayer thus imparting new biophysical/biochemical properties to the membrane. The concept of introducing heterogeneity into the membrane is inspired by nature. Cell membranes comprise a vast class of lipids and proteins, and heterogeneities are known to mediate various cellular processes.

The work by Gettel et al.[144] demonstrates the construction of SLPBs and their use as model membranes for studying obstructed diffusion. The main findings of this work are depicted in **Figure 8**. The substrates were patterned by exposing *n*-octadecyltrichlorosilane covered substrates with a photomask to ozone-generating, short-wavelength UV light (187–254 nm), see schematic in Figure 8A. Two different approaches were developed to form the SLPBs: (1) mixtures of lipid–polymer hybrid vesicles were adsorbed and fused into the patterned substrates, resulting in the formation of a monolayer or a bilayer on the hydrophobic and hydrophilic regions, respectively; and (2) designated surface regions all filled with polymer bilayers were selectively removed and backfilled with lipid bilayers through patterning (Figure 8A).

Interestingly, it was observed that the patterned 1-palmitoyl-2-oleoyl-*sn*-glycero-3-phosphocholine and poly(butadiene-*b*-ethylene oxide) (PBDPEO) onto amphiphilic surfaces remain unmixed (Figure 8B). Lipid patch and polymer patch did not seem to penetrate into each other's region as observed by epifluorescence images (Figure 8B). Such seemingly homogenous distribution of lipid and polymer in each pattern was unexpected because of the small height mismatch between the POPC (≈5 nm thick) bilayer) and the PBDPEO (10–12 nm thick) bilayer. Indeed, phase separation was observed for GUVs made of comparable mixtures.

The observed membrane homogeneity implies an irreversible adsorption of components which was investigated by measuring the lateral diffusion coefficient of POPC in the

**ADVANCED
SCIENCE NEWS**
www.advancedsciencenews.com

**ADVANCED
FUNCTIONAL
MATERIALS**
www.afm-journal.de

Figure 8. A) The process of lipid–polymer supported membrane preparation: deposition of polymer PBDPEO bilayer followed by selective removal and backfilling with lipid POPC bilayer. B) Epifluorescence images of polymer (doped with Texas Red-DHPE) and lipid (doped with NBD-DHPE) bilayers. Scale bar = 100 µm. C) Diffusion constants of probe lipids in hybrid lipid–polymer membranes at different molar ratios. The inset shows the relative diffusion constant of the probe lipids per area fraction of polymers. Reproduced with permission.[144] Copyright 2014, American Chemical Society.

SLPB (Figure 7C). The POPC lateral diffusion was clearly hindered by the presence of PBDPEO on solid supports. The diffusion behavior of POPC in the SLPB clearly differs from the one in freely floating membranes (e.g., GUVs). The mechanism of substrate-mediated fusion of PBDPEO is thought to be responsible for bringing irreversibility in the SLPB, which needs to be further investigated. The implication of this study on SLPBs is that it allows the investigation of obstructed diffusion behavior of transmembrane proteins and lipids in plasma membranes,[148] a process that is still not well understood.

Besides block copolymers, another type of synthetic polymer (dendrimer) was employed to form lipid-dendrimer coassembly structures on solid supports.[149] The hybrid dendrimer/POPC vesicles were exposed to the hydrophilic substrates and incubated in an aqueous environment to allow them to form a well-defined supported bilayer. The fluidity and stability of the membrane could be modulated by controlling the generation (the number of repeated branching cycles) and concentration of the dendrimer. Also, the versatility of the functional end groups in the dendrimers eased the conjugation of biological recognition ligands to the membrane, offering new opportunities to develop powerful sensors.

3.3. Multilayered Phase-Separated Films

In this section, we discuss our recent work on multilayered lipid–polymer hybrid films with nanostructures that enable synergistic and controlled delivery of paclitaxel—a powerful drug that is often challenging to encapsulate and release.[146] We also include very recent (unpublished) structural and chemical composition characterization obtained by photothermal-induced resonance (PTIR, Figure 11) and dynamical characterization obtained by solid-state nuclear magnetic resonance (ssNMR, Figure 12).

Similar to stacked bilayers composed of ternary lipid mixtures,[81] binary lipid–polymer mixtures exhibit a peculiar phase behavior. Lipids and polymers phase separate into lipid-rich and polymer-rich domains, which are in registry across micrometer-thick films, therefore yielding a 3D phase separation. Such 3D segregation provides synergistic permeability of encapsulated hydrophobic drug molecules (Paclitaxel) through the hybrid films.

Figure 9 shows the structural characterization of the self-assembled lipid DPPC–polymer PBDPEO films by confocal laser scanning microscopy (CLSM), AFM, and GISAXS. The coexistence of polymer-rich and lipid-rich domains in the membrane and their out-of-plane alignment were confirmed by CLSM (Figure 9A) and GISAXS (Figure 9B), respectively. As in multilamellar lipid films,[81] like domains did stack up across multiple membrane layers aligning themselves parallel to the substrate. The large height mismatch between lipid and polymer individual layers leads to the formation of extensive phase boundaries, as revealed by AFM topography and phase images (Figure 9C).

Figure 10 shows cumulative drug (paclitaxel) release profiles from neat lipid, neat polymer, and lipid–polymer hybrid films each loaded with paclitaxel (0.02 molar fraction). Interestingly, the hybrid films provided a synergistic permeability compared to single-component films. This striking property was attributed to extensive domain interfaces in the hybrid films that impede paclitaxel crystallization and provide areas for enhanced permeability (i.e., leakiness).
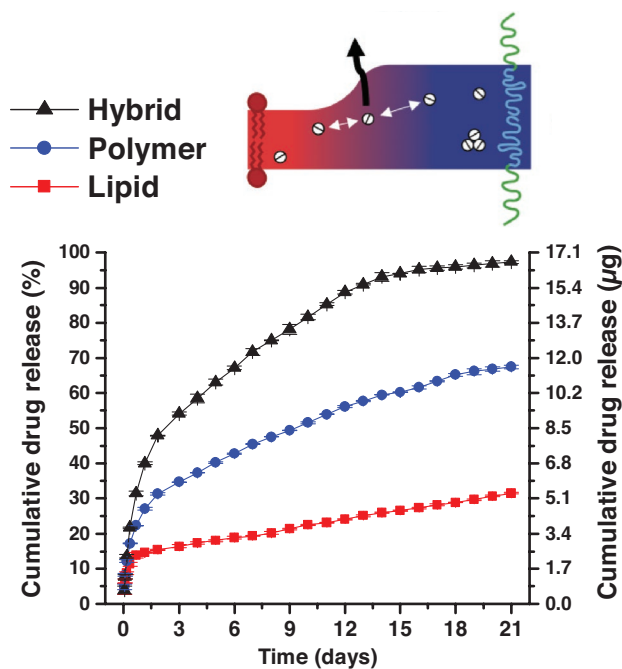
Here, we leverage PTIR experiments to study the distribution of paclitaxel in a paclitaxel loaded (0.05 molar fraction) hybrid DPPC/PBDPEO (1:1 molar ratio) membrane with nanoscale resolution (**Figure 11**). PTIR, also known as AFM-IR, is an emergent technique that combines the high spatial resolution of AFM with the composition specificity of infrared (IR) spectroscopy.[150,151] The proportionality between the PTIR signal and the energy absorbed locally by the sample,[152,153] as in
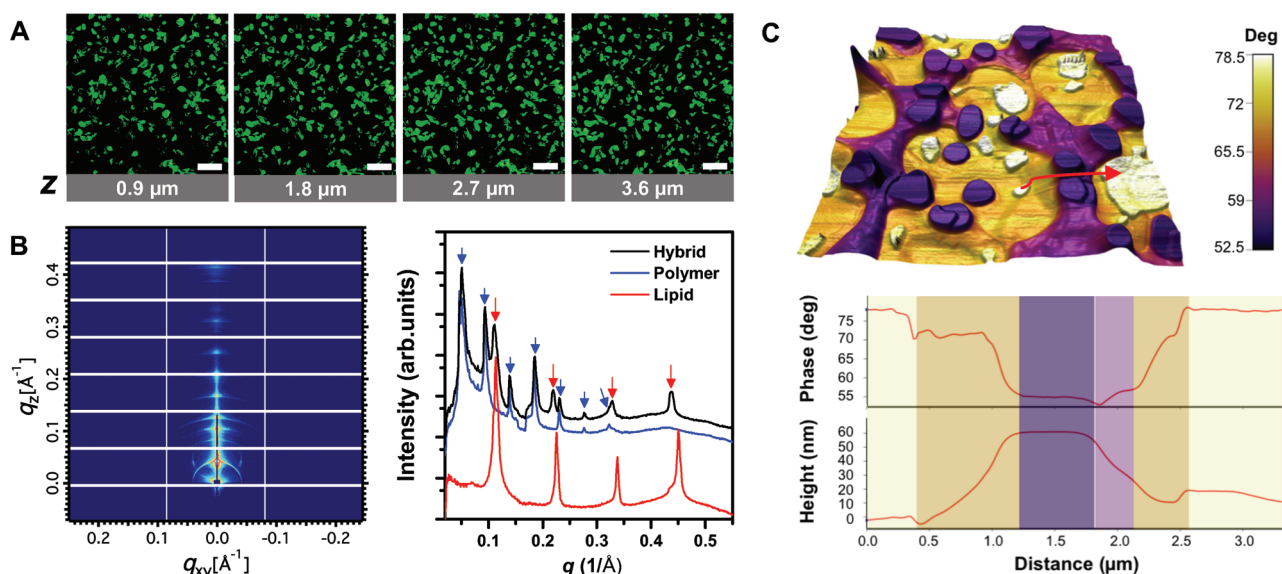
Figure 9. A) Confocal fluorescence microscopy images obtained at different depths (z) inside lipid–polymer hybrid membranes (1:1 molar ratio DPPC:PBDPEO) in bulk water doped with NBD-DPPE (0.001 molar fraction). Binary spatial patterns continue across the membrane normal, suggesting domain alignment across multilamellar membranes. Scale bars = 50 µm. B) GISAXS 2D raw data of hybrid membranes (left) and 1D I(q) profiles of hybrid, lipid, and polymer films (right) obtained at >95% relative humidity. C) AFM phase contrast image overlaid onto pseudo-3D topography of the hybrid membranes (top). Cross-sectional profiles of the phase and topography along the arrow marked in the image (bottom). Reproduced with permission.[146] Copyright 2017, American Chemical Society.

conventional IR spectroscopy, allows material identification at the nanoscale by comparison with far-field IR spectral databases.[151] Recent reviews[150,151] discuss the PTIR working principles and an ever-growing list of applications spanning from

Figure 10. Cumulative release profiles of paclitaxel from 1:1 molar ratio DPPC/PBDPEO hybrid (black triangles), PBD-b-PEO (blue circles), and DPPC (red squares) membranes with 0.02 molar fraction paclitaxel incorporated. Reproduced with permission.[146] Copyright 2017, American Chemical Society.

biology[154,155] to materials science,[156–159] which include studies on the nanoscale distribution of drug–polymer blends.[160,161] Recently, PTIR has been extended to the visible range,[162] enabling measurement of semiconductor bandgap at the nanoscale.[163,164] Furthermore, the development of nanosized picogram-scale probes capable of capturing the sample thermalization dynamics in PTIR experiments has added the ability to measure local thermal conductivity of the sample.[165]

The AFM topography (Figure 11A) and contact resonance frequency (Figure 11B) images of the paclitaxel loaded hybrid film show the phase-separated polymer-rich (higher topography, lower frequency) and lipid-rich (lower topography, higher frequency) domains. Figure 11B suggests that the polymer-rich domains are softer (lower frequency) than the lipid domains because the AFM contact resonance frequency is proportional to the local sample stiffness.[166] This observation corroborates Figure 9C, where the thicker polymer domains display a lower phase value than the lipids due to the lower Young's modulus of the polymer.[167] The Fourier-transform infrared (FTIR) spectra of pure paclitaxel, DPPC, and PBDPEO (Figure 11C) show that the lipid and the polymer have very similar IR spectra (i.e., it is difficult to spectroscopically differentiate them). However, the paclitaxel spectrum shows a few distinct bands that do not overlap with the polymer or the lipid bands, and these peaks, 1645 cm^{-1} (amide I), 1602 cm^{-1} (C=C stretching), 1543 cm^{-1} (amide II), and 1506 cm^{-1} (C=C stretching)[168] were leveraged for the subsequent PTIR experiments. In addition to prominent polymer and lipid bands (≈1730 and ≈1463 cm^{-1}), representative PTIR spectra (Figure 11D) reveal the presence of paclitaxel (see bands at 1650, 1604, and 1506 cm^{-1}) in both the polymer and the lipid domains. Notably the amide I peak of paclitaxel at 1650 cm^{-1} broadens upon the drug's inclusion in the polymer, and broadens and weakens considerably upon the inclusion
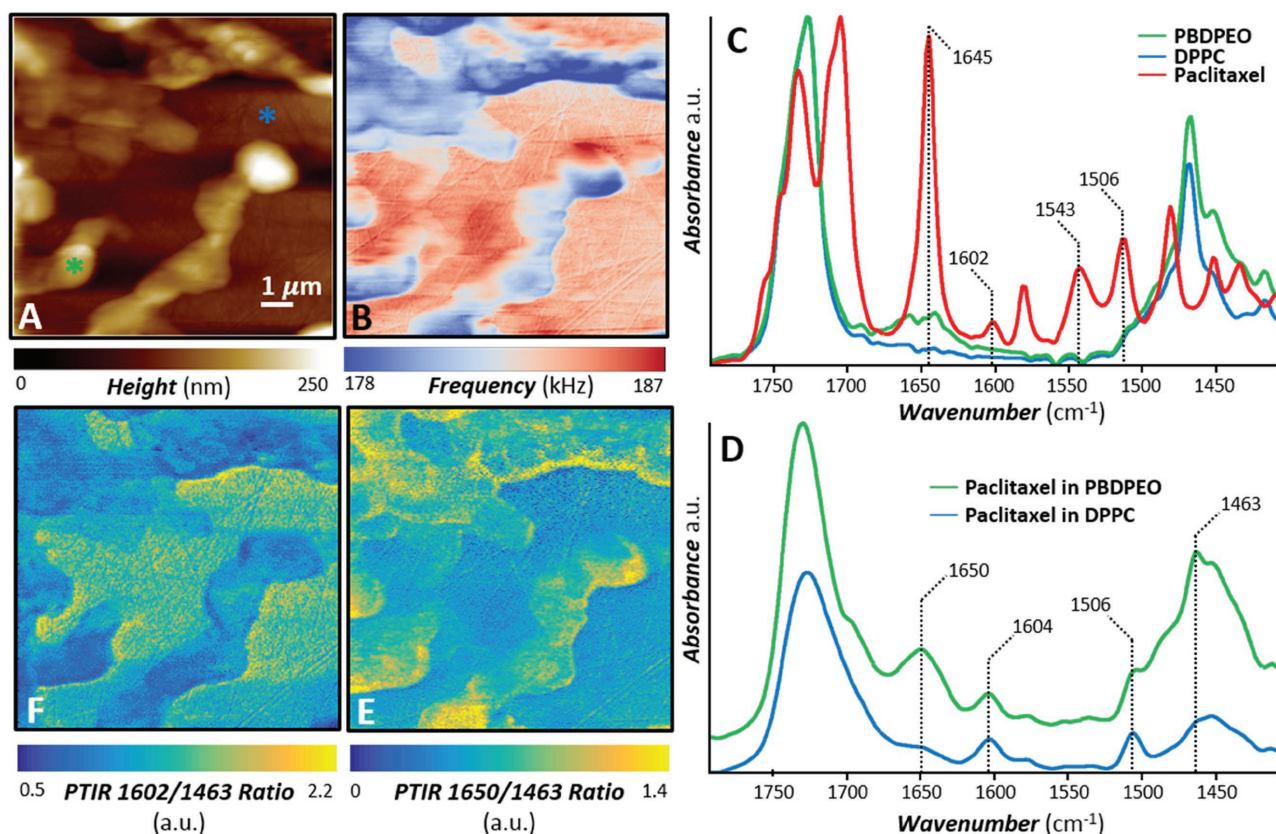
Figure 11. PTIR nanoscale chemical imaging. A) AFM topography image and B) AFM contact frequency image of a paclitaxel loaded (0.05 molar fraction) hybrid 1:1 molar ratio DPPC/PBDPEO film. The features with higher topography and lower contact frequency identify the polymer reach domains. C) Normalized FTIR spectra of PBDPEO (green), DPPC (blue), and paclitaxel (red). D) Characteristic PTIR spectra (displayed with a common intensity scale) obtained in the color-coded positions identified in panel (A). In addition to the polymer and lipid characteristic bands (1463 and 1730 cm^{-1}), a few distinct and characteristic paclitaxel bands indicate that the drug is partitioned in both the polymer and lipid phases. E) PTIR ratio map obtained by dividing the intensity of the 1650 cm^{-1} PTIR map (paclitaxel amide I band) over the 1463 cm^{-1} PTIR map (polymer and lipid band) reveals the heterogeneous distribution of paclitaxel in the polymer-rich phase. F) PTIR ratio map obtained by dividing the intensity of the 1602 cm^{-1} PTIR map (paclitaxel C=C stretching band) over the 1463 cm^{-1} PTIR map (polymer and lipid band).

in the lipid (Figure 11D), perhaps suggesting a stronger interaction between the amide group in the drug and the lipid. In contrast the C=C stretching bands at 1604 and 1506 cm^{-1} are relatively stronger for the paclitaxel incorporated in the lipid phase than in the polymer phase, suggesting a stronger interaction of aromatic groups in paclitaxel with the PBD block in the polymer than with the lipid phase. PTIR chemical maps are obtained by illuminating the sample at a given wavelength while scanning the AFM probe on the sample to enable the visualization of different components. However, it is known that sample locations with higher stiffness, characterized by higher contact resonant frequency (Figure 11B), can provide a little stronger PTIR signal amplitude.[169] Consequently, it is a common practice[169] to analyze a ratio of PTIR maps obtained at two wavelengths (Figure 11 E,F) to cancel out the effect of the sample stiffness variability on the PTIR signal intensity because such effect at each location is wavelength independent. The PTIR ratio map (Figure 11E) of the 1650 cm^{-1} band (amide I of paclitaxel) over the 1463 cm^{-1} band (polymer and lipid) highlights the spatial distribution of paclitaxel in the film and, particularly, the heterogeneous distributions in the polymer-rich phase. Interestingly, it appears that the paclitaxel concentration

is somewhat enhanced along many boundaries between the polymer-rich and lipid-rich domains, thus corroborating our previous hypothesis.[146] The PTIR ratio map (Figure 11F) of the 1602 cm^{-1} band (C=C stretching of paclitaxel) over the 1463 cm^{-1} band (polymer and lipid band) shows that the overall distribution of paclitaxel in the lipid-rich phase is somewhat homogeneous; however, a slightly stronger intensity is observed along some lipid–polymer interfaces, perhaps suggesting again a slightly higher concentration of the drug in these regions.

To investigate the changes in molecular configuration that lipid molecules adopt upon polymer incorporation, we performed ^{13}C ssNMR experiments, which can provide atomically resolved information about molecular conformations and reorientational dynamics. The results are presented in **Figure 12**. Three different ^{13}C NMR measurements were combined: direct polarization (DP), cross-polarization (CP),[170] and refocused insensitive nuclei enhanced by polarization transfer (INEPT).[171] The two different methods of ^{1}H–^{13}C polarization transfer used for enhancing the ^{13}C signals (CP and INEPT) complement each other as they respond differently to the reorientational dynamics of C−H bonds (which can be quantified with the correlation time τ_C and order parameter S_{CH}[172]).
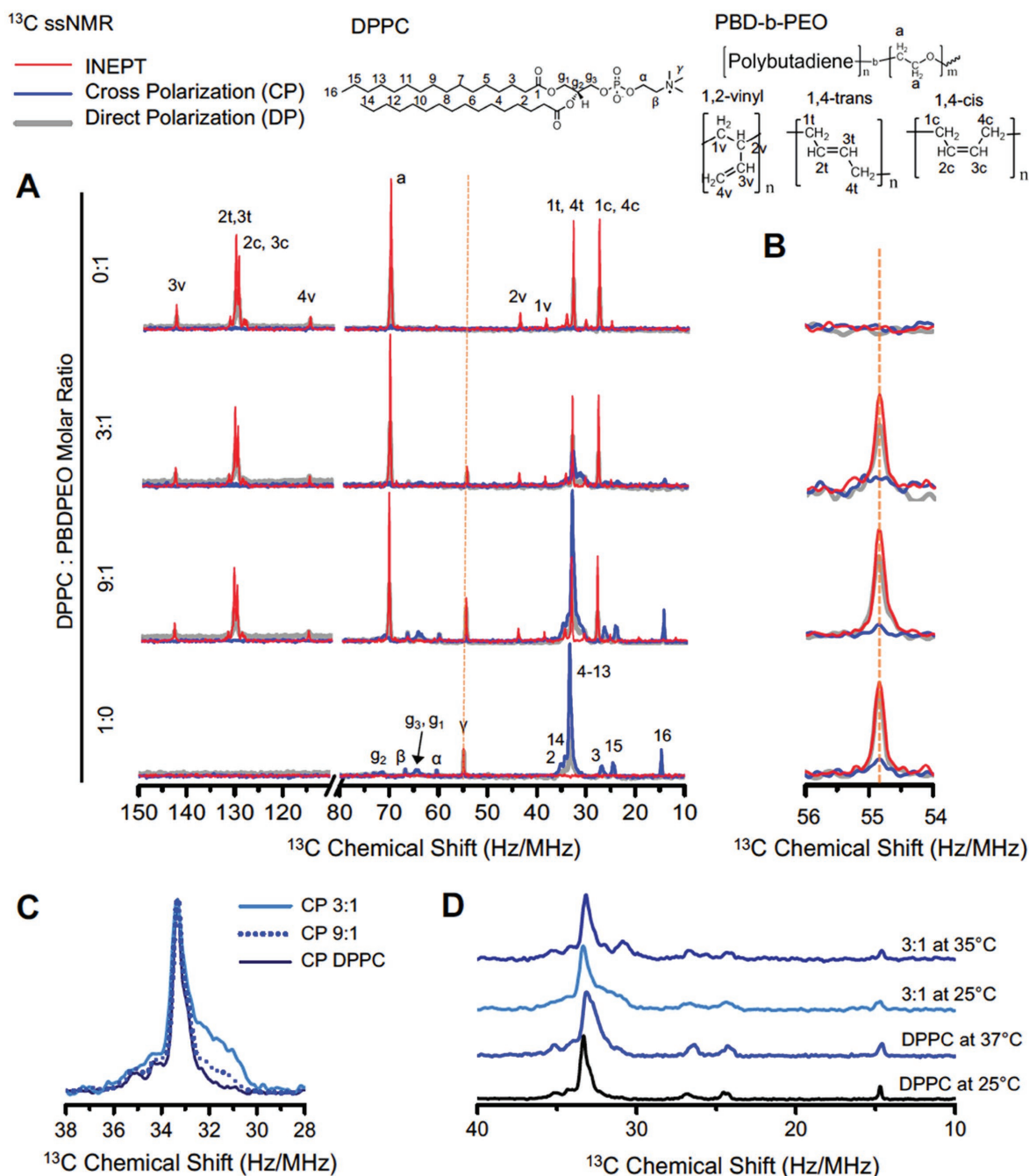
Figure 12. 13C solid-state NMR spectra of lipids, polymers, and lipid–polymer hybrids. Top: Molecular structure of lipid DPPC and polymer PBDPEO with the carbon atom labeling. A) The combined DP (gray lines)–CP (blue lines)–INEPT (red lines) sets of DPPC (bottom), 9:1 molar ratio DPPC/ PBDPEO, 3:1 molar ratio DPPC/PBDPEO (middle), and PBDPEO (top). All samples were measured at 25 °C. The spectrum of DPPC exhibits dominant CP signals compared to INEPT while that of PBDPEO presents the opposite trend: strong INEPT signals without CP. The peaks at 54.8 Hz MHz^{-1} (denoted by dashed lines) are enlarged in (B) to emphasize the relative signal amplitudes of DP, CP, and INEPT. Resonances at 54.8 Hz MHz^{-1} correspond to the DPPC headgroup moiety "γ." As PBDPEO is incorporated into DPPC membranes, CP of headgroup "γ" decreases along with increased INEPT to DP ratios, indicating that the lipid headgroup becomes fluidic upon polymer incorporation. C) The CP spectra of DPPC (black, solid) and 9:1 molar ratio DPPC/PBDPEO (blue, dotted) and 3:1 molar ratio DPPC/PBDPEO (skyblue, solid). The spectra are normalized to equal intensity of the 33 Hz MHz^{-1} shift which is characteristic of the acyl chains adapting all-trans conformations. The significant line broadening is observed in the regions of 30–33 Hz MHz^{-1} for DPPC/PBDPEO hybrids, which can be attributed to the perturbed lipid acyl chain packing in the presence of polymer yielding a distribution of different conformations. D) The CP spectra of DPPC and 3:1 molar ratio DPPC/PBDPEO are compared at two different temperatures, 25 and 37 °C. Spectra are labeled by compound name. The broad peak of DPPC/PBDPEO differs from that of DPPC even at elevated temperature. The appearance of carbon peak at 31 Hz MHz^{-1} from 3:1 molar ratio DPPC/PBDPEO at 37 °C reveals that some portions of acyl chains in the hybrids already transform into liquid-like conformations below the Tm of DPPC (41 °C).

**ADVANCED
SCIENCE NEWS**

www.advancedsciencenews.com

**ADVANCED
FUNCTIONAL
MATERIALS**

www.afm-journal.de

Solids ($\tau_C > 0.1$ μs and/or $|S_{CH}| > 0.5$) yield intense CP signals but lack INEPT signals, while anisotropic liquids ($\tau_C < 10$ ns and $0.05 < |S_{CH}| < 0.2$) give comparable CP and INEPT signals.[173,174] For isotropic liquids ($\tau_C < 10$ ns and $|S_{CH}| < 0.01$), strong INEPT with vanishing CP is observed.[173,174] Consequently, the INEPT to CP signals ratios can readily provide qualitative information about the molecular segment mobility.

Figure 12A shows the DP-CP-INEPT set of ^{13}C spectra of DPPC (bottom), DPPC/PBDPEO hybrids (middle), and PBDPEO (top). The DP, CP, and INEPT spectra were superimposed and color coded in gray, blue, and red, respectively. The peaks were assigned based on single-component control samples of DPPC and PBDPEO, in agreement with the previous works.[175–177] The polarization transfer efficiency for DPPC (25 °C) was $I_{CP} > I_{DP} \gg I_{INEPT} \approx 0$ as expected for a solid gel phase[178] ($T_{m, DPPC} = 41$ °C). An opposite trend was found for PBDPEO, suggesting that polymer carbon chains are liquid-like and mobile. DPPC/PBDPEO hybrids display peaks associated with DPPC and PBDPEO which seem to be the simple overlap of two phases at first glance. A closer look, however, reveals two characteristic differences between hybrids and single-component samples (see the magnified 54–56 Hz MHz^{-1} region corresponding to the lipid headgroup moiety (γ in Figure 12B). The relative intensities of DP, CP, and INEPT of the carbon γ clearly show changes in lipid headgroup dynamics when the polymer is present. For DPPC, the polarization transfer efficiency follows the order $I_{INEPT} \approx I_{DP} \gg I_{CP} > 0$ but as the PBDPEO content increases the relative intensities become $I_{INEPT} > I_{DP} \gg I_{CP} \approx 0$. Such increase in INEPT/DP ratios and the absence of CP signals[173,174] indicate the segment γ in DPPC which has some degree of anisotropy in its pure phase but it undergoes complete isotropic reorientation when PBDPEO coexists. This is a clear indication that the hybrid polymer–lipid membranes do not consist of two completely phase-separated sets of polymers and lipids.

Other notable differences between pure and hybrid phases are shown in Figure 12C,D. Figure 12C compares normalized CP scans of DPPC and DPPC/PBDPEO hybrids in the 28–38 Hz MHz^{-1} range where the acyl chain peak positions indicate whether the hydrocarbon chains are in an *all-trans* conformation or contain *gauche* conformations. The broad peak centered at 33 Hz MHz^{-1} originates from the central segment of the acyl chains (C$_{4–13}$) in *all-trans* conformation[178] whereas liquid acyl chains with a distribution of *trans*- and *gauche* conformations show the peak at 31 Hz MHz^{-1}.[179] Interestingly, DPPC/PBDPEO hybrids exhibit the acyl chain peak with a broad shoulder in comparison to DPPC, indicating that some portions of the acyl chains are in not only *all-trans* but acquire a distribution of *trans*- and *gauche* conformations. Such behavior on the conformational distribution of the acyl chains can only be understood as a perturbation of lipid chain packing due to the coexistence of polymer molecules within the membrane.

To further investigate the characteristics of different chain conformations in DPPC/PBDPEO hybrids, we compared DPPC and DPPC/PBDPEO hybrids at 37 °C at which DPPC is in the ripple phase (P$'_\beta$). The ripple phase is characterized by periodically undulated bilayers with troughs and ridges.[180] Figure 12D shows the 37 °C data obtained for DPPC where an upfield shift of the C$_{4–13}$ peak with a broadened shoulder can be observed.

Notably, the peak shape clearly differs from that obtained for DPPC/PBDPEO at 25 °C, indicating that the broadened C$_{4–13}$ peak of DPPC/PBDPEO is not just a simple result of the DPPC phase transition from the gel to ripple (L$'_\beta$ to P$'_\beta$). Continuous resonances of DPPC/PBDPEO in the 31–33 Hz MHz^{-1} region rather reflect a wide distribution of chain conformations in the DPPC acyl chains. At 37 °C, the shoulder of the main acyl chain peak at 33 Hz MHz^{-1} of DPPC/PBDPEO separates out to another peak centered at 31 Hz MHz^{-1}, indicating that an elevated temperature causes some of the hydrocarbon chains to acquire a *liquid*-like distribution of conformations. Taken all together, the DPPC acyl chains go through conformational changes when PBDPEO molecules are incorporated and such distribution of different conformations in DPPC/PBDPEO differs from the ones seen in pure DPPC phases (L$'_\beta$ or P$'_\beta$). In AFM phase imaging (Figure 9C), we observed gradual AFM topography and phase changes between lipid domains and polymer domains, likely indicating the presence of mixed domains where lipid and polymer molecules coexist. In line with the AFM phase data, the continuous resonances from 31 to 33 Hz MHz^{-1} of DPPC/PBDPEO may be a result of the wide range of (or gradual conformational changes in) DPPC molecular states that are sensitive to the presence of PBDPEO molecules.

In this work, we have demonstrated the use of multilayered lipid–polymer hybrid films for substrate-mediated drug delivery applications. Intralayer and interlayer domain ordering of hybrid films has implications for accurate control of the permeation behavior of embedded solutes through the films.

4. Summary and Outlook

Until recently, lipid films have been mostly used as model systems to mimic cell membranes. The aim of this review is to show that supported lipid-based materials have the potential to catalyze many substrate-mediated applications such as drug/gene delivery, biomimetic energy conversion, and sensing.

Lipids are biocompatible and possess the capability to self-assemble into various phases both in nature and artificial systems. Lipid molecules are the structural motifs that comprise cell membranes, indicating that lipid self-assembled structures are versatile in terms of adapting to external stimuli/environmental changes. These characteristics should be very compelling arguments to investigate and exploit lipid materials beyond cell membrane models. One can envisage biocompatible lipid films becoming instrumental to the development of new medical devices requiring susceptibility in response to specific stimuli. Importantly, when lipids self-assemble onto a support, interesting structural features are observed such as specific orientation and stacking. Multicomponent lipid mixtures phase separate into coexisting domains and those domains stack up in registry, resulting in columnar alignment across lipid multilayers.[81]

Lipid polymorphism as seen in the bulk is mostly retained for lipids prepared as supported films with the added complexity of the preferred orientation of the polymorphic phases. A theoretical framework to understand the orientation of lipid films has been established by Latypova et al.[124] and Richardson et al.[119] in the context of thermodynamic minimization for

**ADVANCED
SCIENCE NEWS**
www.advancedsciencenews.com

**ADVANCED
FUNCTIONAL
MATERIALS**
www.afm-journal.de

surface energy. Further understanding on substrate effects will allow the engineering of on-demand structures and orientation. Substrate modification based on recent surface functionalization technologies is expected to play a key role in dictating the structure of lipid films (from a few layers adjacent to the substrate propagating to the entire film thickness).

Artificial transplants, stents, scaffolds for tissue engineering, surface-based drug/gene delivery, and macroscale drug delivery devices all necessitate biocompatible and functional coatings. A few, original studies that employ lipid materials in those applications have already demonstrated their great utility as reservoirs of several therapeutic cargos and their ability to release active species in response to stimuli. It should be noted that phase transformations in lipid films are fast and involve the conversion between systems that have dramatically distinct nanostructures, permeability, and diffusion behaviors, a feature that is less prominent in polymer systems.

Because lipids are so adaptable, however, this characteristic also constitutes a bottleneck for their application. One important aspect is the lack of mechanical robustness and stability when interfaced with hard materials or harsh environments. A clear future direction in this field will be the development of mechanically robust lipid-based materials capable of retaining the biocompatibility and the capacity to quickly transform into different structures as a function of specific environmental cues. There have been a few efforts to address this challenge by incorporating additional components such as lipid–silica or copolymers. The key in those processes is to maintain the functionality of the systems, in particular of the bioactive agents incorporated into the lipid-based films. We argue that one of the most promising developments in the field will revolve around composite lipid–polymer hybrid materials, which, as the literature cited in this review suggests, is an emerging field that has experienced rapid growth over the past 5 years. Concurrent self-assembly of lipids and polymers into the same membrane results in hybrid membranes that show interesting and diverse phase behavior, spanning from homogeneous mixing to micro- and macrophase separation. Inherent advantages provided by polymer systems include ease of composition engineering, tunable mechanical stability, and membrane permeability. These properties are expected to synergistically cooperate with the advantages provided by lipid systems such as biocompatibility and responsiveness to external stimuli. Incorporation of distinct functional species (hydrophobic/ hydrophilic drugs, nanoparticles, or proteins) could be carefully directed to be coassembled in certain membrane domains and released at different time points. Such location selectivity of functional components is one advantage conferred by introducing in-plane heterogeneities into the lipid membranes. The fact that those heterogeneities align in registry across a wide space field offers an opportunity to control active species concentration by stacking layers at different thicknesses. Although the nanostructure and the orientation of the phases can be somewhat modulated and predicted there is still an enduring lack of control over the size, shape, and distribution of in-plane phase-separated membrane domains which should be addressed in future research. With the exception of a few studies conducted in our laboratory shown here, multilayered hybrid lipid–polymer films are essentially an unexplored

material system that deserves further exploration. In addition, phase behavior studies of hybrid films have been limited to planar membrane systems although a rich polymorphism akin to lipid-only or polymer-only systems should be expected. Structural and chemical diversities brought by the lipid–polymer hybrid films would broaden the application space of lipid-based films. To meet the rapidly rising demand for coatings, matrices, and scaffold materials in biotechnology applications, we expect to anticipate that more research efforts will be devoted to lipid-based films.

5. Experimental Section

In Sections 2.3.2 and 3.3, lipid-based films were prepared by standard methodologies based on the dissolution of lipids and polymers in an organic solvent followed by spin coating and solvent evaporation onto solid substrates. Details of materials used, sample preparation, as well as SAXS and AFM methodologies can be consulted in the following papers.[16,146]

Fourier-Transform Infrared and Photothermal-Induced Resonance: Samples for FTIR and PTIR experiments were prepared using spin-coating method as described above. Details of materials used and sample preparation for PTIR can be consulted in the Supporting Information. FTIR spectra were acquired with a commercial spectrometer in total internal reflection geometry (4 cm^{-1} spectral resolution). Each spectrum is the average of 128 consecutive scans. PTIR spectra and images were obtained with a commercial PTIR instrument interfaced with a quantum cascade laser tunable from 1934 cm^{-1} (5.17 μm) to 1136 cm^{-1} (8.80 μm). The PTIR laser illuminates the sample from the top at ≈20° angle from the sample plane. Commercially available 450 μm long and 50 μm wide gold-coated silicon AFM probes with a nominal spring constant between 0.07 and 0.4 N m^{-1} were used for all the PTIR experiments. A paclitaxel-loaded (0.05 molar fraction) hybrid lipid–polymer film was spin coated onto ZnS flat substrate to minimize the background absorption contribution of the substrate.

PTIR spectra and images were obtained by tuning the laser repetition rate to resonantly excite[181] the AFM cantilever second bending oscillation mode. In contrast to the original implementation of the resonance enhanced PTIR method that used lock-in detection at the cantilever resonant frequency,[181] we leveraged a phase lock-in loop to better account for resonant frequency shifts as a function of location (or time) due to variations in the sample-probe interactions. PTIR spectra were obtained by tuning the laser at intervals of 2 cm^{-1}. Up to six spectra were acquired and averaged for each tip location, and smoothed by considering two adjacent points. AFM topography and PTIR maps were acquired simultaneously illuminating the sample at constant wavelength. Because the sample mechanical properties are known to influence the amplitude of the PTIR response,[169] throughout the manuscript we use PTIR absorption map ratios, to cancel out the effect of the local mechanical properties of the sample on the data.

Polarization Transfer Solid-State Nuclear Magnetic Resonance: Samples for NMR experiments were prepared using thin film hydration method.[182] Details of materials used and sample preparation can be consulted in the Supporting Information. NMR experiments were performed on a Bruker Avance-II 500 spectrometer[183] (Karlsruhe, Germany) equipped with a 4 mm ^{13}C/^{31}P/^{1}H Efree probe and a 11.7 T magnet, giving resonance frequencies of 500 MHz for ^{1}H and 125 MHz for ^{13}C. 1D ^{1}H direct-polarization spectra and ^{13}C DP, cross-polarization,[170] and insensitive nuclei enhanced by polarization transfer[171] spectra were measured at 5 kHz magic-angle spinning and temperatures from 298 to 316 K. The samples were equilibrated for 1 h at each temperature before measurements. The ^{13}C spectra were acquired with 31.25 kHz spectral width and 100 ms acquisition time under 48 kHz two-pulse phase-modulated ^{1}H decoupling.[184] The ^{13}C chemical shifts were calibrated by referring to the signal of solid α-glycine at

43.67 Hz MHz^{-1}.[185] The CP acquisition parameters were contact time 1 ms, 80 kHz ^{13}C nutation frequency, and linear ramp of ^{1}H nutation frequency from 72 to 88 kHz, while the delays in the INEPT sequence were $t = 1.2$ ms and $t' = 1.8$ ms. All 90° and 180° pulses were applied at 80 kHz nutation frequency. Accumulation of 1280 transients at a recycle delay of 5 s yielded a measurement time of 107 min per spectrum. 1D NMR spectra were processed with a commercial data analysis package with the following processing parameters; the line broadening factor was set to be 10 Hz, and the size of real spectrum (SI) was 8192 and the size of fid (TD) was 3120.

Conflict of Interest

The authors declare no conflict of interest.

[1] K. Simons, W. L. C. Vaz, *Annu. Rev. Biophys. Biomol. Struct.* **2004**, *33*, 269.

[2] G. van Meer, D. R. Voelker, G. W. Feigenson, *Nat. Rev. Mol. Cell Biol.* **2008**, *9*, 112.

[3] Y. Tu, F. Peng, A. Adawy, Y. Men, L. K. E. A. Abdelmohsen, D. A. Wilson, *Chem. Rev.* **2016**, *116*, 2023.

[4] G. Gregoriadis, B. E. Ryman, *Biochem. J.* **1971**, *124*, 58P.

[5] G. Gregoriadis, *FEBS Lett.* **1973**, *36*, 292.

[6] T. M. Allen, P. R. Cullis, *Adv. Drug Delivery Rev.* **2013**, *65*, 36.

[7] J. C. Kraft, J. P. Freeling, Z. Wang, R. J. Y. Ho, *J. Pharm. Sci.* **2014**, *103*, 29.

[8] L. K. Tamm, H. M. McConnell, *Biophys. J.* **1985**, *47*, 105.

[9] E. T. Castellana, P. S. Cremer, *Surf. Sci. Rep.* **2006**, *61*, 429.

[10] R. P. Richter, R. Bérat, A. R. Brisson, *Langmuir* **2006**, *22*, 3497.

[11] P. R. Cullis, B. de Kruijff, *Biochim. Biophys. Acta* **1979**, *559*, 399.

[12] P. R. Cullis, M. J. Hope, C. P. Tilcock, *Chem. Phys. Lipids* **1986**, *40*, 127.

[13] J. M. Seddon, R. H. Templer, in *Handbook of Biolgical Physics* (Eds: R. Lipowsky, E. Sackmann), Elsevier, Amsterdam **1995**, pp. 97–160.

[14] B. Ericsson, P. O. Eriksson, J. E. Löfroth, S. Engström, in *Polymeric Drugs and Drug Delivery System* (Eds: R. L. Dunn, R. M. Ottenbrite), American Chemical Society, Washington, DC **1991**, pp. 251–265.

[15] W.-K. Fong, T. Hanley, B. J. Boyd, *J. Controlled Release* **2009**, *135*, 218.

[16] M. Kang, C. Leal, *Adv. Funct. Mater.* **2016**, *26*, 5610.

[17] C. Leal, N. F. Bouxsein, K. K. Ewert, C. R. Safinya, *J. Am. Chem. Soc.* **2010**, *132*, 16841.

[18] H. Kim, C. Leal, *ACS Nano* **2015**, *9*, 10214.

[19] J. J. Vallooran, S. Handschin, S. M. Pillai, B. N. Vetter, S. Rusch, H.-P. Beck, R. Mezzenga, *Adv. Funct. Mater.* **2016**, *26*, 181.

[20] M. Kang, G. Huang, C. Leal, *Soft Matter* **2014**, *10*, 8846.

[21] B. J. Boyd, W.-K. Fong, in *Self-Assembled Supramolecular Architectures: Lyotropic Liquid Crystals* (Eds: N. Garti, P. Somasundaran, R. Mezzenga), John Wiley & Sons, Inc., Hoboken, NJ **2012**, pp. 257–288.

[22] X. Guo, J. Andrew MacKay, F. C. Szoka, *Biophys. J.* **2003**, *84*, 1784.

[23] M. Wadsäter, J. Barauskas, T. Nylander, F. Tiberg, *Soft Matter* **2013**, *9*, 8815.

[24] T. Nylander, O. Soltwedel, M. Ganeva, C. Hirst, J. Holdaway, M. Y. Arteta, M. Wadsäter, J. Barauskas, H. Frielinghaus, O. Holderer, *J. Phys. Chem. B* **2017**, *121*, 2705.

[25] M. Rittman, H. Amenitsch, M. Rappolt, B. Sartori, B. M. D. O'Driscoll, A. M. Squires, *Langmuir ACS J. Surf. Colloids* **2013**, *29*, 9874.

[26] A. C. R. Grayson, R. S. Shawgo, A. M. Johnson, N. T. Flynn, Y. Li, M. J. Cima, R. Langer, *Proc. IEEE* **2004**, *92*, 6.

[27] Y.-H. Joung, *Int. Neurourol. J.* **2013**, *17*, 98.

[28] J. El-Ali, P. K. Sorger, K. F. Jensen, *Nature* **2006**, *442*, 403.

[29] M. Cheng, G. Cuda, Y. Bunimovich, M. Gaspari, J. Heath, H. Hill, C. Mirkin, A. Nijdam, R. Terracciano, T. Thundat, *Curr. Opin. Chem. Biol.* **2006**, *10*, 11.

[30] C. N. LaFratta, D. R. Walt, *Chem. Rev.* **2008**, *108*, 614.

[31] R. B. Shmueli, D. G. Anderson, J. J. Green, *Expert Opin. Drug Delivery* **2010**, *7*, 535.

[32] C.-H. K. Wang, S. H. Pun, *Trends Biotechnol.* **2011**, *29*, 119.

[33] D. R. Jung, R. Kapur, T. Adams, K. A. Giuliano, M. Mrksich, H. G. Craighead, D. L. Taylor, *Crit. Rev. Biotechnol.* **2001**, *21*, 111.

[34] R. Ogaki, M. Alexander, P. Kingshott, *Mater. Today* **2010**, *13*, 22.

[35] Y. Lei, S. Yang, M. Wu, G. Wilde, *Chem. Soc. Rev.* **2011**, *40*, 1247.

[36] J. Berthier, P. Silberzan, *Microfluidics for Biotechnology*, Artech House, Boston, MA **2006**.

[37] P. N. Nge, C. I. Rogers, A. T. Woolley, *Chem. Rev.* **2013**, *113*, 2550.

[38] A. F. Oliveira, A. C. S. N. Pessoa, R. G. Bastos, L. G. de la Torre, *Biotechnol. Prog.* **2016**, *32*, 1372.

[39] C. J. Bettinger, Z. Bao, *Polym. Int.* **2010**, *59*, 563.

[40] M. Irimia-Vladu, *Chem. Soc. Rev.* **2014**, *43*, 588.

[41] C. J. Kearney, D. J. Mooney, *Nat. Mater.* **2013**, *12*, 1004.

[42] A. N. Zelikin, *ACS Nano* **2010**, *4*, 2494.

[43] V. Kiessling, M. K. Domanska, D. Murray, C. Wan, L. K. Tamm, in *Wiley Encyclopedia of Chemical Biology*, (Ed: T. P. Begley), John Wiley & Sons, Inc., Hoboken, NJ **2008**.

[44] J. Jackman, W. Knoll, N.-J. Cho, *Materials* **2012**, *5*, 2637.

[45] Y. F. Dufrêne, G. U. Lee, *Biochim. Biophys. Acta, Biomembr.* **2000**, *1509*, 14.

[46] J. F. Nagle, S. Tristram-Nagle, *Biochim. Biophys. Acta* **2000**, *1469*, 159.

[47] S. Tristram-Nagle, J. F. Nagle, *Chem. Phys. Lipids* **2004**, *127*, 3.

[48] J.-F. Le Meins, C. Schatz, S. Lecommandoux, O. Sandre, *Mater. Today* **2013**, *16*, 397.

[49] M. Schulz, A. Olubummo, W. H. Binder, *Soft Matter* **2012**, *8*, 4849.

[50] M. Schulz, W. H. Binder, *Macromol. Rapid Commun.* **2015**, *36*, 2031.

[51] Y. Liu, B. Liu, Z. Nie, *Nano Today* **2015**, *10*, 278.

[52] S. J. Johnson, T. M. Bayerl, D. C. McDermott, G. W. Adam, A. R. Rennie, R. K. Thomas, E. Sackmann, *Biophys. J.* **1991**, *59*, 289.

[53] C. A. Keller, B. Kasemo, *Biophys. J.* **1998**, *75*, 1397.

[54] M.-P. Mingeot-Leclercq, M. Deleu, R. Brasseur, Y. F. Dufrêne, *Nat. Protoc.* **2008**, *3*, 1654.

[55] M. L. Kraft, *Science* **2006**, *313*, 1948.

[56] K. B. Blodgett, *J. Am. Chem. Soc.* **1935**, *57*, 1007.

ADVANCED
Science News

www.advancedsciencenews.com

ADVANCED
FUNCTIONAL
MATERIALS

www.afm-journal.de

[57] A. Ulman, *An Introduction to Ultrathin Organic Films: From Langmuir–Blodgett to Self-Assembly*, Academic Press, Boston, MA **1991**.

[58] P. S. Cremer, S. G. Boxer, *J. Phys. Chem. B* **1999**, *103*, 2554.

[59] R. Richter, A. Mukhopadhyay, A. Brisson, *Biophys. J.* **2003**, *85*, 3035.

[60] T. K. Lind, M. Cárdenas, H. P. Wacklin, *Langmuir* **2014**, *30*, 7259.

[61] E. Kalb, S. Frey, L. K. Tamm, *Biochim. Biophys. Acta* **1992**, *1103*, 307.

[62] M. L. Wagner, L. K. Tamm, *Biophys. J.* **2000**, *79*, 1400.

[63] L. Kam, S. G. Boxer, *J. Biomed. Mater. Res.* **2001**, *55*, 487.

[64] D. E. Minner, P. Rauch, J. Käs, C. A. Naumann, *Soft Matter* **2014**, *10*, 1189.

[65] S. Vafaei, S. R. Tabaei, K. H. Biswas, J. T. Groves, N.-J. Cho, *Adv. Healthcare Mater.* **2017**, *6*, 1700243.

[66] J. T. Groves, *Science* **1997**, *275*, 651.

[67] K. S. Phillips, Q. Cheng, *Anal. Chem.* **2005**, *77*, 327.

[68] J. M. Moran-Mirabal, J. B. Edel, G. D. Meyer, D. Throckmorton, A. K. Singh, H. G. Craighead, *Biophys. J.* **2005**, *89*, 296.

[69] Y. Suzuki, M. Endo, H. Sugiyama, *Nat. Commun.* **2015**, *6*, 8052.

[70] W. Knoll, C. W. Frank, C. Heibel, R. Naumann, A. Offenhäusser, J. Rühe, E. K. Schmidt, W. W. Shen, A. Sinner, *Rev. Mol. Biotechnol.* **2000**, *74*, 137.

[71] T. Salditt, *J. Phys. Condens. Matter* **2005**, *17*, R287.

[72] G. Pompeo, M. Girasole, A. Cricenti, F. Cattaruzza, A. Flamini, T. Prosperi, J. Generosi, A. Congiu Castellano, *Biochim. Biophys. Acta, Biomembr.* **2005**, *1712*, 29.

[73] L. Perino-Gallice, G. Fragneto, U. Mennicke, T. Salditt, F. Rieutord, *Eur. Phys. J. E: Soft Matter Biol. Phys.* **2002**, *8*, 275.

[74] B. Nowak, M. Paulus, J. Nase, P. Salmen, P. Degen, F. J. Wirkert, V. Honkimäki, M. Tolan, *Langmuir* **2016**, *32*, 2638.

[75] T. Hønger, K. Mortensen, J. H. Ipsen, J. Lemmich, R. Bauer, O. G. Mouritsen, *Phys. Rev. Lett.* **1994**, *72*, 3911.

[76] Y. Ma, S. K. Ghosh, S. Bera, Z. Jiang, C. M. Schlepütz, E. Karapetrova, L. B. Lurio, S. K. Sinha, *Phys. Chem. Chem. Phys.* **2016**, *18*, 1225.

[77] D. Constantin, C. Ollinger, M. Vogel, T. Salditt, *Eur. Phys. J. E: Soft Matter Biol. Phys.* **2005**, *18*, 273.

[78] G. S. Gavelis, S. Hayakawa, R. A. White III, T. Gojobori, C. A. Suttle, P. J. Keeling, B. S. Leander, *Nature* **2015**, *523*, 204.

[79] S. C. Payne, C. A. Bartlett, A. R. Harvey, S. A. Dunlop, M. Fitzgerald, *Invest. Opthalmol. Visual Sci.* **2012**, *53*, 6093.

[80] C. Laule, I. M. Vavasour, S. H. Kolind, D. K. B. Li, T. L. Traboulsee, G. R. W. Moore, A. L. MacKay, *Neurotherapeutics* **2007**, *4*, 460.

[81] L. Tayebi, Y. Ma, D. Vashaee, G. Chen, S. K. Sinha, A. N. Parikh, *Nat. Mater.* **2012**, *11*, 1074.

[82] B. Bechinger, *Nat. Mater.* **2012**, *11*, 1005.

[83] D. Bald, J. Kruip, M. Rögner, *Photosynth. Res.* **1996**, *49*, 103.

[84] M. Pribil, M. Labs, D. Leister, *J. Exp. Bot.* **2014**, *65*, 1955.

[85] F. O. Schmitt, R. S. Bear, K. J. Palmer, *J. Cell. Comp. Physiol.* **1941**, *18*, 31.

[86] B. B. Geren, *Exp. Cell Res.* **1954**, *7*, 558.

[87] H. W. Trissl, C. Wilhelm, *Trends Biochem. Sci.* **1993**, *18*, 415.

[88] D. K. Hartline, *Neuron Glia Biol.* **2008**, *4*, 153.

[89] M. H. Brodnitz, *J. Agric. Food Chem.* **1968**, *16*, 994.

[90] A. Reis, C. M. Spickett, *Biochim. Biophys. Acta, Biomembr.* **2012**, *1818*, 2374.

[91] J. H. Crowe, L. M. Crowe, J. F. Carpenter, A. S. Rudolph, C. A. Wistrom, B. J. Spargo, T. J. Anchordoguy, *Biochim. Biophys. Acta, Biomembr.* **1988**, *947*, 367.

[92] U. Mennicke, T. Salditt, *Langmuir* **2002**, *18*, 8172.

[93] G. Gupta, S. Iyer, K. Leasure, N. Virdone, A. M. Dattelbaum, P. B. Atanassov, G. P. López, *ACS Nano* **2013**, *7*, 5300.

[94] G. R. Heath, M. Li, I. L. Polignano, J. L. Richens, G. Catucci, P. O'Shea, S. J. Sadeghi, G. Gilardi, J. N. Butt, L. J. C. Jeuken, *Biomacromolecules* **2016**, *17*, 324.

[95] S. Matosevic, B. M. Paegel, *Nat. Chem.* **2013**, *5*, 958.

[96] D. H. Murray, L. K. Tamm, V. Kiessling, *J. Struct. Biol.* **2009**, *168*, 183.

[97] M. Chung, R. D. Lowe, Y.-H. M. Chan, P. V. Ganesan, S. G. Boxer, *J. Struct. Biol.* **2009**, *168*, 190.

[98] X. Han, A. S. Achalkumar, M. R. Cheetham, S. D. A. Connell, B. R. G. Johnson, R. J. Bushby, S. D. Evans, *ChemPhysChem* **2010**, *11*, 569.

[99] L. A. Lautscham, C. Y. Lin, V. Auernheimer, C. A. Naumann, W. H. Goldmann, B. Fabry, *Biomaterials* **2014**, *35*, 3198.

[100] M. K. I. Khan, L. H. Mujawar, M. A. I. Schutyser, K. Schroën, R. Boom, *Food Bioprocess Technol.* **2013**, *6*, 3047.

[101] Y. Zhu, A. Negmi, J. Moran-Mirabal, *Membranes* **2015**, *5*, 385.

[102] O. A. Nafday, T. W. Lowry, S. Lenhert, *Small* **2012**, *8*, 1021.

[103] B. Sironi, T. Snow, C. Redeker, A. Slastanova, O. Bikondoa, T. Arnold, J. Klein, W. H. Briscoe, *Soft Matter* **2016**, *12*, 3877.

[104] G. R. Heath, M. Li, H. Rong, V. Radu, S. Frielingsdorf, O. Lenz, J. N. Butt, L. J. C. Jeuken, *Adv. Funct. Mater.* **2017**, *1606265*.

[105] C. H. Lee, H. Kim, D. V. Harburg, G. Park, Y. Ma, T. Pan, J. S. Kim, N. Y. Lee, B. H. Kim, K.-I. Jang, S.-K. Kang, Y. Huang, J. Kim, K.-M. Lee, C. Leal, J. A. Rogers, *NPG Asia Mater.* **2015**, *7*, e227.

[106] S. L. Perry, S. G. Neumann, T. Neumann, K. Cheng, J. Ni, J. R. Weinstein, D. V. Schaffer, M. Tirrell, *AIChE J.* **2013**, *59*, 3203.

[107] D. Steer, M. Kang, C. Leal, *Nanotechnology* **2017**, *28*, 142001.

[108] P. A. Janmey, J. P. Winer, J. W. Weisel, *J. R. Soc. Interface* **2009**, *6*, 1.

[109] T. R. Thatiparti, A. J. Shoffstall, H. A. von Recum, *Biomaterials* **2010**, *31*, 2335.

[110] M. L. Macdonald, R. E. Samuel, N. J. Shah, R. F. Padera, Y. M. Beben, P. T. Hammond, *Biomaterials* **2011**, *32*, 1446.

[111] N. J. Shah, M. N. Hyder, J. S. Moskowitz, M. A. Quadir, S. W. Morton, H. J. Seeherman, R. F. Padera, M. Spector, P. T. Hammond, *Sci. Transl. Med.* **2013**, *5*, 191ra83.

[112] A. Solanki, S. Shah, P. T. Yin, K.-B. Lee, *Sci. Rep.* **2013**, *3*, 1553.

[113] S. N. Bailey, R. Z. Wu, D. M. Sabatini, *Drug Discovery Today* **2002**, *7*, S113.

[114] D. B. Wheeler, A. E. Carpenter, D. M. Sabatini, *Nat. Genet.* **2005**, *37*, S25.

[115] T. Neumann, S. Gajria, M. Tirrell, L. Jaeger, *J. Am. Chem. Soc.* **2009**, *131*, 3440.

[116] T. Neumann, S. Gajria, N. F. Bouxsein, L. Jaeger, M. Tirrell, *J. Am. Chem. Soc.* **2010**, *132*, 7025.

[117] T. Fukushima, *Biomaterials* **2004**, *25*, 5491.

[118] M. Rittman, M. Frischherz, F. Burgmann, P. G. Hartley, A. Squires, *Soft Matter* **2010**, *6*, 4058.

[119] S. J. Richardson, P. A. Staniec, G. E. Newby, N. J. Terrill, J. M. Elliott, A. M. Squires, W. T. Góźdź, *Langmuir* **2014**, *30*, 13510.

[120] R. H. Templer, J. M. Seddon, N. A. Warrender, A. Syrykh, Z. Huang, R. Winter, J. Erbes, *J. Phys. Chem. B* **1998**, *102*, 7251.

[121] J. Bender, M. B. Ericson, N. Merclin, V. Iani, A. Rosén, S. Engström, J. Moan, *J. Controlled Release* **2005**, *106*, 350.

[122] M. Kang, H. Kim, C. Leal, *Curr. Opin. Colloid Interface Sci.* **2016**, *26*, 58.

[123] H. Kim, Z. Song, C. Leal, *Proc. Natl. Acad. Sci. USA* **2017**, *114*, 10834.

[124] L. Latypova, W. T. Góźdź, P. Pierański, *Langmuir* **2014**, *30*, 488.

[125] Y. Rancon, J. Charvolin, *J. Phys. Chem.* **1988**, *92*, 2646.

[126] M. E. Vigild, K. Almdal, K. Mortensen, I. W. Hamley, J. P. A. Fairclough, A. J. Ryan, *Macromolecules* **1998**, *31*, 5702.

[127] A. M. Squires, S. Akbar, M. E. Tousley, Y. Rokhlenko, J. P. Singer, C. O. Osuji, *Langmuir* **2015**, *31*, 7707.

[128] S. Akbar, J. M. Elliott, M. Rittman, A. M. Squires, *Adv. Mater.* **2013**, *25*, 1160.

[129] S. J. Richardson, M. R. Burton, P. A. Staniec, I. S. Nandhakumar, N. J. Terrill, J. M. Elliott, A. M. Squires, *Nanoscale* **2016**, *8*, 2850.

[130] C. Leal, K. K. Ewert, N. F. Bouxsein, R. S. Shirazi, Y. Li, C. R. Safinya, *Soft Matter* **2013**, *9*, 795.

[131] W. Sun, J. J. Vallooran, W.-K. Fong, R. Mezzenga, *J. Phys. Chem. Lett.* **2016**, *7*, 1507.

[132] *Amphiphilic Block Copolymers: Self-Assembly and Applications* (Eds: B. Lindman, P. Alexandridis), Elsevier, Amsterdam **2000**.

[133] A. Blanazs, S. P. Armes, A. J. Ryan, *Macromol. Rapid Commun.* **2009**, *30*, 267.

[134] H. Bermúdez, D. A. Hammer, D. E. Discher, *Langmuir* **2004**, *20*, 540.

[135] Z. Song, H. Kim, X. Ba, R. Baumgartner, J. S. Lee, H. Tang, C. Leal, J. Cheng, *Soft Matter* **2015**, *11*, 4091.

[136] T. Ruysschaert, A. F. P. Sonnen, T. Haefele, W. Meier, M. Winterhalter, D. Fournier, *J. Am. Chem. Soc.* **2005**, *127*, 6242.

[137] J. Nam, P. A. Beales, T. K. Vanderlick, *Langmuir* **2011**, *27*, 1.

[138] J. Nam, T. K. Vanderlick, P. A. Beales, *Soft Matter* **2012**, *8*, 7982.

[139] M. Chemin, P.-M. Brun, S. Lecommandoux, O. Sandre, J.-F. Le Meins, *Soft Matter* **2012**, *8*, 2867.

[140] D. Chen, M. M. Santore, *Soft Matter* **2015**, *11*, 2617.

[141] T. P. T. Dao, F. Fernandes, E. Ibarboure, K. Ferji, M. Prieto, O. Sandre, J.-F. Le Meins, *Soft Matter* **2017**, *13*, 627.

[142] T. P. T. Dao, A. Brûlet, F. Fernandes, M. Er-Rafik, K. Ferji, R. Schweins, J.-P. Chapel, A. Fedorov, M. Schmutz, M. Prieto, O. Sandre, J.-F. Le Meins, *Langmuir* **2017**, *33*, 1705.

[143] S. K. Lim, A. Wong, H.-P. M. De Hoog, P. Rangamani, A. Parikh, M. Nallani, S. Sandin, B. Liedberg, *Soft Matter* **2017**, *13*, 1107.

[144] D. L. Gettel, J. Sanborn, M. A. Patel, H.-P. de Hoog, B. Liedberg, M. Nallani, A. N. Parikh, *J. Am. Chem. Soc.* **2014**, *136*, 10186.

[145] J. Kowal, D. Wu, V. Mikhalevich, C. G. Palivan, W. Meier, *Langmuir* **2015**, *31*, 4868.

[146] M. Kang, B. Lee, C. Leal, *Chem. Mater.* **2017**, *29*, 9120

[147] A. Olubummo, M. Schulz, B.-D. Lechner, P. Scholtysek, K. Bacia, A. Blume, J. Kressler, W. H. Binder, *ACS Nano* **2012**, *6*, 8713.

[148] T. K. Fujiwara, K. Iwasawa, Z. Kalay, T. A. Tsunoyama, Y. Watanabe, Y. M. Umemura, H. Murakoshi, K. G. N. Suzuki, Y. L. Nemoto, N. Morone, A. Kusumi, *Mol. Biol. Cell* **2016**, *27*, 1101.

[149] S. S. Hinman, C. J. Ruiz, Y. Cao, M. C. Ma, J. Tang, E. Laurini, P. Posocco, S. Giorgio, S. Pricl, L. Peng, Q. Cheng, *ACS Appl. Mater. Interfaces* **2017**, *9*, 1029.

[150] A. Centrone, *Annu. Rev. Anal. Chem.* **2015**, *8*, 101.

[151] A. Dazzi, C. B. Prater, *Chem. Rev.* **2017**, *117*, 5146.

[152] A. Dazzi, F. Glotin, R. Carminati, *J. Appl. Phys.* **2010**, *107*, 124519.

[153] B. Lahiri, G. Holland, A. Centrone, *Small* **2013**, *9*, 439.

[154] F. S. Ruggeri, G. Longo, S. Faggiano, E. Lipiec, A. Pastore, G. Dietler, *Nat. Commun.* **2015**, *6*, 7831.

[155] A. Dazzi, R. Prazeres, F. Glotin, J. M. Ortega, M. Al-Sawaftah, M. de Frutos, *Ultramicroscopy* **2008**, *108*, 635.

[156] A. M. Katzenmeyer, J. Canivet, G. Holland, D. Farrusseng, A. Centrone, *Angew. Chem., Int. Ed.* **2014**, *53*, 2852.

[157] J. Chae, B. Lahiri, A. Centrone, *ACS Photonics* **2016**, *3*, 87.

[158] L. Gong, D. B. Chase, I. Noda, J. Liu, D. C. Martin, C. Ni, J. F. Rabolt, *Macromolecules* **2015**, *48*, 6197.

[159] E. Strelcov, Q. Dong, T. Li, J. Chae, Y. Shao, Y. Deng, A. Gruverman, J. Huang, A. Centrone, *Sci. Adv.* **2017**, *3*, e1602165.

[160] H. S. Purohit, L. S. Taylor, *Mol. Pharm.* **2015**, *12*, 1623.

[161] B. Van Eerdenbrugh, M. Lo, K. Kjoller, C. Marcott, L. S. Taylor, *Mol. Pharm.* **2012**, *9*, 1459.

[162] A. M. Katzenmeyer, G. Holland, K. Kjoller, A. Centrone, *Anal. Chem.* **2015**, *87*, 3154.

[163] J. Chae, Q. Dong, J. Huang, A. Centrone, *Nano Lett.* **2015**, *15*, 8114.

[164] Y. Yoon, J. Chae, A. M. Katzenmeyer, H. P. Yoon, J. Schumacher, S. An, A. Centrone, N. Zhitenev, *Nanoscale* **2017**, *9*, 7771.

[165] J. Chae, S. An, G. Ramer, V. Stavila, G. Holland, Y. Yoon, A. A. Talin, M. Allendorf, V. A. Aksyuk, A. Centrone, *Nano Lett.* **2017**, *17*, 5587.

[166] D. G. Yablon, A. Gannepalli, R. Proksch, J. Killgore, D. C. Hurley, J. Grabowski, A. H. Tsou, *Macromolecules* **2012**, *45*, 4363.

[167] S. N. Magonov, V. Elings, M.-H. Whangbo, *Surf. Sci.* **1997**, *375*, L385.

[168] G. Socrates, *J. Chem. Educ.* **1995**, *72*, A93.

[169] D. E. Barlow, J. C. Biffinger, A. L. Cockrell-Zugell, M. Lo, K. Kjoller, D. Cook, W. K. Lee, P. E. Pehrsson, W. J. Crookes-Goodson, C.-S. Hung, L. J. Nadeau, J. N. Russell, *Analyst* **2016**, *141*, 4848.

[170] A. Pines, M. G. Gibby, J. S. Waugh, *Chem. Phys. Lett.* **1972**, *15*, 373.

[171] G. A. Morris, R. Freeman, *J. Am. Chem. Soc.* **1979**, *101*, 760.

[172] B. Halle, H. Wennerström, *J. Chem. Phys.* **1981**, *75*, 1928.

[173] A. Nowacka, N. A. Bongartz, O. H. S. Ollila, T. Nylander, D. Topgaard, *J. Magn. Reson.* **2013**, *230*, 165.

[174] A. Nowacka, P. C. Mohr, J. Norrman, R. W. Martin, D. Topgaard, *Langmuir* **2010**, *26*, 16848.

[175] T. Mavromoustakos, E. Theodoropoulou, D.-P. Yang, *Biochim. Biophys. Acta, Biomembr.* **1997**, *1328*, 65.

[176] L. B. Canto, G. L. Mantovani, E. R. deAzevedo, T. J. Bonagamba, E. Hage, L. A. Pessan, *Polym. Bull.* **2006**, *57*, 513.

[177] R. Mahou, C. Wandrey, *Polymers* **2012**, *4*, 561.

[178] V. Jagalski, R. Barker, D. Topgaard, T. Günther-Pomorski, B. Hamberger, M. Cárdenas, *Biochim. Biophys. Acta, Biomembr.* **2016**, *1858*, 2827.

[179] W. L. Earl, D. L. VanderHart, *Macromolecules* **1979**, *12*, 762.

[180] M. Rappolt, G. Rapp, *Eur. Biophys. J.* **1996**, *24*, 381.

[181] F. Lu, M. Jin, M. A. Belkin, *Nat. Photonics* **2014**, *8*, 307.

[182] D. D. Lasic, *Liposomes: From Physics to Applications*, Elsevier, Amsterdam **1993**.

[183] The equipment used in this paper requires the identification of a commercial product and its supplier. The inclusion of such information should in no way be constructed as indicating that such product or supplier is endorsed by NIST or is recommended by NIST or that is necessarily the best material for the purpose described.

[184] A. E. Bennett, C. M. Rienstra, M. Auger, K. V. Lakshmi, R. G. Griffin, *J. Chem. Phys.* **1995**, *103*, 6951.

[185] S. Hayashi, K. Hayamizu, *Bull. Chem. Soc. Jpn.* **1991**, *64*, 685.